

Multi-core parallel tempering Bayeslands for basin and landscape evolution

Rohitash Chandra^{1,2}, R. Dietmar Müller¹, Danial Azam¹, Ratneel Deo¹,
Nathaniel Butterworth³, Tristan Salles¹, Sally Cripps⁴

¹EarthByte Group, School of Geosciences, University of Sydney, NSW 2006, Sydney, Australia

²Centre for Translational Data Science, University of Sydney, NSW 2006, Sydney, Australia

³Sydney Informatics Hub, University of Sydney, NSW 2006, Sydney, Australia

⁴School of Mathematics and Statistics, University of Sydney, NSW 2006, Sydney, Australia

Key Points:

- Landscape evolution
- Bayesian inference
- Parallel tempering
- Badlands
- Bayeslands

arXiv:1806.10939v2 [physics.geo-ph] 20 Jul 2019

Abstract

The Bayesian paradigm is becoming an increasingly popular framework for estimation and uncertainty quantification of unknown parameters in geo-physical inversion problems. Badlands is a basin and landscape evolution forward model for simulating topography evolution at a large range of spatial and time scales. Our previous work presented Bayeslands that used the Bayesian paradigm to make inference for unknown parameters in the Badlands model using Markov chain Monte Carlo (MCMC) sampling. Bayeslands faced challenges in convergence due to multi-modal posterior distributions in the selected parameters of Badlands. Parallel tempering is an advanced MCMC method suited for irregular and multi-modal posterior distributions. In this paper, we extend Bayeslands using parallel tempering (PT-Bayeslands) with high performance computing to address previous limitations in parameter space exploration in the context of the computationally expensive Badlands model. Our results show that PT-Bayeslands not only reduces the computation time, but also provides an improvement of the sampling for multi-modal posterior distributions. This provides an improvement over Bayeslands which used single chain MCMC that face difficulties in convergence and can lead to misleading inference. This motivates its usage in large-scale basin and landscape evolution models.

1 Introduction

Understanding landscape evolution, and the associated accumulation of sediments in basins, is limited by increasingly sparse data back through geological time. Recent developments in landscape evolution models (LEMs) [Coulthard, 2001], such as the basin and landscape dynamics (Badlands) model feature responses to surface uplift and subsidence over a large range of spatial scales, and track sediments from source to sink [Salles and Hardiman, 2016; Salles et al., 2017, 2018a]. Badlands also has the capability to create synthetic basin stratigraphies. LEMs depend on uncertain initial and boundary conditions [Scott and Zhang, 1990]; such as the initial topography, sea level, precipitation, and rock lithology and erodibility [Godard et al., 2006; Rejman et al., 1998]. Quantifying uncertainty surrounding these initial conditions and how the topography changes over time is an incredibly difficult task.

To make inference about the parameters that govern landscape evolution, we need to constrain the model by fusing information from various sources in a probabilistic model. The sources of information include underlying equations that govern LEMs to represent geophysical processes, observed data such as present day topography, stratigraphy in sedimentary basins, and previous research which could be denoted as expert knowledge [Salles et al., 2018a].

The Bayesian framework provides a logically consistent mechanism for fusing information from various sources to provide meaningful inference for unknown parameters in models. The prior distribution is a mechanism to incorporate information from previous research and expert opinion, and the likelihood is a mechanism to incorporate information from data to sample from the posterior distribution that represents the unknown parameter [Tarantola, 2006]. The ability to fuse information from many sources in a principled fashion has made Bayesian inference an increasingly popular choice for the estimation and uncertainty quantification of parameters in complex models [Robert and Casella, 2011; Mosegaard and Vestergaard, 1991; Rocca et al., 2009; Sen and Stoffa, 2013; Gallagher et al., 2009]. More specifically, there is some work that employs Bayesian inversion methodologies for landscape evolution based forward models for specific applications. Initial work was done by [Roberts and White, 2010] who used Monte Carlo inverse modeling of river profiles to estimate uplift rate histories using African examples. [Fox et al., 2014] reviewed uplift and erosion rate history of the Bergell intrusion from the inversion of low temperature thermochronometric data and [Goren et al., 2014] focused on distinguishing tectonics from fluvial topography using formal linear inversion

with applications to the Inyo Mountains, California. [Fox *et al.*, 2015] investigated the rate of Andean Plateau uplift using reversible jump MCMC inversion of river profiles.

Although Bayesian inversion has become popular in geophysics in the past few decades [Grandis *et al.*, 1999; Malinverno, 2002; Mosegaard and Tarantola, 1995; Sambridge and Mosegaard, 2002; Sambridge, 1999], estimating the posterior distribution is often non-trivial. The posterior distributions can be multimodal, exhibit discontinuities and is usually not available in closed form; hence, Markov chain Monte Carlo (MCMC) sampling methods are used to estimate it and crafting proposal distributions to explore these distributions is very difficult [Gallagher *et al.*, 2009].

The Metropolis-Hastings algorithm [Hastings, 1970; Metropolis *et al.*, 1953; Chib and Greenberg, 1995] is a popular MCMC method to obtain iterations from a distribution that cannot be sampled directly. In the Metropolis-Hastings algorithm, the current state in the Markov chain, is moved to a new state via a transition kernel. This transition kernel consists of a proposal distribution and an acceptance probability. Given some regularity conditions, this acceptance probability is constructed so that the Markov chain will converge to the posterior (stationary) distribution, irrespective of the proposal distribution. However, the proposal distribution does effect the rate at which the chain converges. A poorly chosen proposal distribution can result in an acceptance probability close to zero and the chain will not converge in a timely fashion. Information about the gradient of the posterior may help with the construction of better proposal distributions [Neal *et al.*, 2011; Hoffman and Gelman, 2014; Girolami and Calderhead, 2011]; however, in geophysical forward models, gradients are often unavailable or too computationally expensive to obtain. In situations such as these, parallel tempering Markov Chain Monte Carlo (PT-MCMC) [Marinari and Parisi, 1992; Geyer and Thompson, 1995] offers the best chance of convergence.

PT-MCMC is well suited for exploring multi-modal distributions by running replicas of the Markov chains in parallel. In PT-MCMC, the replicas converge to different stationary distributions which effectively smooth out the local modes that exist in the posterior. The parameters in replicas are allowed to swap with each other, ensuring that the target chain will contain draws from other local maxima. In addition, parallel computing based implementation of PT-MCMC can reduce the computational burden associated with complex forward models such as Badlands [Zhang *et al.*, 2007; Vrugt *et al.*, 2006; Mills *et al.*, 1992]. The potential for PT-MCMC in geoscience has been demonstrated for complex multimodal problems [Sambridge, 2013; Sen and Stoffa, 1996; Maraschini and Foti, 2010; Sen and Stoffa, 2013; Scalzo *et al.*, 2019]. Although recent implementations of PT-MCMC with gradient-based proposals have shown promising performance [Chandra *et al.*, 2019a], they are not feasible for the Badlands model because gradients are unavailable from the model.

Although MCMC methods with random-walk proposals are feasible for models that do not provide gradients, they are inefficient and likely to get stuck in local modes [Neal, 1996]. In our previous work [Chandra *et al.*, 2019b], we presented the Bayeslands framework that used single chain random-walk Metropolis Hastings as a proposal distribution to obtain draws from the posterior distributions of interest. The method did not use parallel computing, and hence referred to as single chain Bayeslands (SC-Bayeslands), hereafter. SC-Bayeslands demonstrated that even in low dimensional settings, the posterior surfaces of parameters exhibited highly irregular features, such as multimodality and discontinuities, making sampling difficult.

In this paper, we present a multi-core parallel tempering Bayeslands (PT-Bayeslands) that features uncertainty quantification and estimation of selected parameters for basin and landscape evolution. We investigate a number of issues such as sampling multi-modal

posterior distributions, proposal distributions, computational time and prediction quality of Badlands. We apply our technique to simulated data and real-world topographies.

2 Background and Related Work

2.1 Badlands

Over the last decades, many numerical models have been proposed to simulate how the Earth surface has evolved over geological time scales in response to different driving forces such as tectonics or climatic variability [Whipple and Tucker, 2002; Tucker and Hancock, 2010; Salles and Duclaux, 2015; Campforts et al., 2017; Adams et al., 2017]. These models combine empirical data and conceptual methods into a set of mathematical equations that can be used to reconstruct landscape evolution and associated sediment fluxes [Howard et al., 1994; Hobbey et al., 2011]. They are currently used in many research fields such as hydrology, soil erosion, hillslope stability and general landscape studies.

We use Badlands [Salles and Hardiman, 2016; Salles, 2016; Salles et al., 2018b] to simulate regional to continental sediment deposition and associated sedimentary basin architecture [Salles et al., 2017, 2018c]. In its basic formulation, the Earth surface elevation change, denoted by $\frac{\partial z}{\partial t}$; where z is the elevation and t refers to time in years related to the interaction of three types of processes: the tectonic uplift rate (U), the incision rate by rivers (I) and the hillslope processes (D).

$$\frac{\partial z}{\partial t} = U - I + D \quad (1)$$

In this study, fluvial incision rates and predicted sediment transport in rivers are solved using the stream-power law (SPL) [Stock and Montgomery, 1999; Harel et al., 2016]. SPL relates the erosion rate I to the product of mean annual net precipitation rate (\bar{P}), drainage area (A), and local river gradient (S) and takes the form:

$$I = k(\bar{P}A)^\gamma S^\lambda \quad (2)$$

where, k is an erodibility coefficient that depends on lithology and climate, while γ (< 2) and λ (< 4) are positive exponents [Chen et al., 2014] that mostly depend on catchment hydrology and the nature of the dominant erosional mechanism [Whipple and Tucker, 2002]. Despite its simplicity, Equation 2 reproduces many of the characteristic features of mountainous landscapes, where detachment-limited erosion regime dominates [Tucker and Hancock, 2010]. κ varies by several orders of magnitude not only based on lithology, climate, sedimentary flux or river channel width but also with the chosen values of γ and λ .

In addition to overland flow, semi-continuous processes of soil displacement are accounted for using a linear diffusion law commonly referred to as soil creep [Tucker and Hancock, 2010]:

$$D = \delta \nabla^2 z \quad (3)$$

where δ is the diffusion coefficient. This transport rate depends linearly on topographic gradient and encapsulates in a simple formulation the processes operating on superficial sedimentary layers.

2.2 SC-Bayeslands

The posterior distributions of parameters in geophysical inversions problems are notoriously difficult to sample [Sambridge, 1999]. They are high dimensional, multimodal and sometimes exhibit discontinuities. SC-Bayeslands provides a framework for travers-

ing the posterior distribution of selected parameters of the Badlands model. In our previous work [Chandra *et al.*, 2019b], we found that SC-Bayeslands had difficulty in convergence due to multimodal posterior distributions. In the experiments, we used two problems, namely the synthetic crater (Cr) and the continental margin (CM) problem to demonstrate effectiveness of Bayeslands. We considered estimation of *precipitation* and *erodibility*, which are the key parameters in the Badlands model.

Figures 1 and 2 show examples of the posterior distributions for precipitation and erodibility, while fixing all other parameters, for the Cr and CM problems, respectively. The Cr log-posterior surface in Figure 1 is smooth but has a clearly defined ridge, which SC-Bayeslands has difficulty exploring. We note that our previous work [Chandra *et al.*, 2019b] showed that different combinations of precipitation and erodibility gave rise to visually indistinguishable topography for both the Cr and CM problem. Figure 2 has a clear global maximum but also several local maxima. Here, unless the chain has a starting value near this global maximum, it is unlikely that it would be found by SC-Bayeslands.

Furthermore, the problems (Cr and CM) used in SC-Bayeslands took computational time of a few seconds and hence it was possible to take thousands of samples for convergence. There is impracticability in applying the SC-Bayeslands for landscape evolution problems that have a computational time of several minutes to few hours, hence parallel computing is needed.

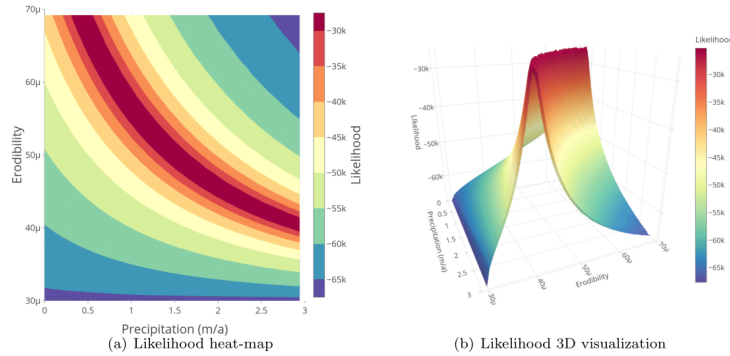


Figure 1: Panels (a) and (b) are a heat map and a surface plot of the log posterior surface of the Cr as function of precipitation, ρ , and erodibility, ϵ [Chandra *et al.*, 2019b].

2.3 Parallel tempering MCMC

PT-MCMC features an ensemble of replicas (samplers) that are executed in parallel with the ability to explore multi-modal posterior distributions [Geyer and Thompson, 1995]. Parallel tempering carries out an exchange of parameters in neighbouring replicas during sampling that is helpful in escaping local minima. In other words, the Markov chains in the ensemble of replicas have stationary distributions which are equal to (up to a proportionality constant) $p(\theta|\mathbf{D})^\beta$, where $\beta \in [0, 1]$ and is known as the *temperature* of the replica. A replica which has a temperature of $\beta = 0$ has a stationary distribution which is uniform while one which has a temperature $\beta = 1$ corresponds to a stationary distribution which is the posterior $p(\theta|\mathbf{D})$. This means that the replica where $\beta \ll 1$ have local maxima which are less separated, and therefore, replicas with smaller values of β are less likely to get stuck in a local minima and thus explore a larger region. The replicas with higher values of β typically explore local regions. The choice of the tem-

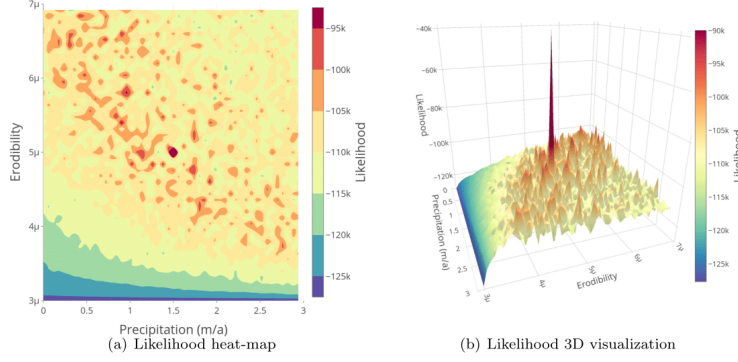


Figure 2: Panels (a) and (b) are a heat map and a surface plot of the log posterior surface of the CM problem as function of precipitation, ρ , and erodibility, ϵ . The true values have a clear peak in the log-posterior (precipitation=1.5 m/a, erodibility= $5e^{-6}$), however many sub-optimal peaks (marked in red) for this parameter pair exist [Chandra *et al.*, 2019b].

perature ladder and number of replicas governs the computational efficiency of the PT-MCMC and is the subject of much research. For instance, [Kone and Kofke, 2005; Patriksson and van der Spoel, 2008] describe an efficient method of finding the temperature ladder, and [Miasojedow *et al.*, 2013] proposed a method for attentively adapting the temperature ladder based on the performance.

The other feature of parallel tempering is their feasibility of implementation in multi-core or parallel computing architectures. In multi-core implementation, factors such as inter-process communications need to be considered during the exchange between the neighboring replicas [Lamport, 1986]. Effective communication strategies between the processes that execute the respective replicas needs to be made in order to reduce the overhead of processes waiting for others. Hence, a decentralized implementation of parallel tempering is presented that eliminates global synchronization and reduces the overhead caused by inter-process communication in exchange of solutions between the chains that run in parallel cores [Li *et al.*, 2009]. Parallel tempering has also been implemented in a distributed volunteer computing network where computers belonging to the general public are used with help of multi-threading and graphic processing units (GPUs) [Karimi *et al.*, 2011]. The implementation with Field Programmable Gate Arrays (FPGAs) that has massive parallelism capabilities resulted in much better performance than multi-core and GPU implementations [Mingas *et al.*, 2017]. In terms of applications, other studies have efficiently implemented parallel tempering via multi-core architectures for exploration of Earth’s resources [Reid *et al.*, 2013].

3 Methodology

3.1 Synthetic topography data

Badlands is a forward stratigraphic model that takes at time $t = 0$, an initial topography denoted by $\mathbf{D}_0 = (D_{s_1 0}, \dots, D_{s_n 0})$; where $D_{s_i 0}$ is the elevation at site s_i at time $t = 0$, for $i = 1, \dots, n$, given n years. The parameters in Badlands model are denoted by θ that are used to produce a series of topographies, $\mathbf{D}_0, \mathbf{D}_1, \dots, \mathbf{D}_T$. We assume that the final topography \mathbf{D}_T , is the only topography to compare with the ground-truth topography. Therefore, the task of making inference about the landscape evolution over time is very difficult.

The four key input parameters represented by θ include precipitation (ρ), rock erodibility (k), and the contribution of rain and slope on erodibility denoted by m-value (μ) and n-value (ν), respectively. Additional parameters depending on the nature of the landscape evolution problem include surface (γ) and marine (β) which govern coastal landscapes. In problems where mountain building processes are involved, the tectonic uplift (u) parameter is utilized. The relationship between these variables and landscape evolution is given by Equations 1- 3. The function that maps the initial topography and these parameters to the final topography (time $t = T$) is denoted by $\mathbf{f}_T(\mathbf{D}_0, \theta) = (f_{T,s_1}(\mathbf{D}_0, \theta), \dots, f_{T,s_n}(\mathbf{D}_0, \theta))$, where f_{T,s_i} is the elevation at time T for site s_i , for $i = 1, \dots, n$.

Different landscape evolution trajectories could lead to the same final topography, and to constrain the number of possible trajectories requires additional sources of information. One source of information is the history of sediment erosion/deposition at various locations. We denote the sediment erosion/deposition at time t by $\mathbf{z}_t = (z_{s_1 t}, \dots, z_{s_J t})$; where $z_{s_j, t}$ is the sediment erosion/deposition at site s_j for $j = 1, \dots, J$. We define another function that maps \mathbf{D}_0 and θ to sediment erosion/deposition by $\mathbf{g}_t(\mathbf{D}_0, \theta) = (g_{s_1 t}(\mathbf{D}_0, \theta), \dots, g_{s_m t}(\mathbf{D}_0, \theta))$, for $t = 1, \dots, T$.

In order to test the proposed methodology, we first use Badlands to create synthetic ground-truth topography data for two synthetic and a real-world landscape evolution problem. We use the present day topography as the initial model topography. We use Badlands to model landscape and basin evolution given values for selected parameters (Table 2) and a specified time T_{max} (Table 1) given by number of years to simulate the ground-truth data for topography and sediment erosion/deposition. We refer to the selected problems as Synthetic-Crater (Cr), Synthetic-Mountain (Mt) and Continental Margin (CM) problems. The first two problems have a synthetic initial topography (hence the name) while the third uses a real landscape, in the North-Eastern region of the South Island in New Zealand as its initial topography (Figure 3). In all the problems, the Badlands model takes selected parameter values together with the initial topographies to produce final topographies. The initial and final topographies for all three problems are shown in Figure 4. We note that Cr and CM has been adapted from examples of the Badlands model ¹, and also used in our previous work [Chandra *et al.*, 2019b].

These three problems were chosen to highlight the impact of different parameters on the final topography. In the Cr problem the parameters are precipitation ρ , rock erodibility k , the contribution of rain and slope on erodibility γ and λ respectively, so that $\theta_{Cr} = (\rho, k, \mu, \nu)$. The Mt problem starts off with a much simpler initial topography, but features the impact of tectonic uplift, u as well as all the four inputs in Cr problem, so that $\theta_{Mt} = (\rho, k, \mu, \nu, u)$. The CM problem does not feature tectonic uplift; however, since the location covers coastal region, it includes parameters which model the impact of the surface and marine environment on landscape evolution, so that $\theta_{CM} = (\rho, k, \mu, \nu, \beta, \lambda)$.

The parameter μ is particularly important in that it describes the sensitivity of a tectonically active mountain belt to changes in precipitation or tectonic accretion. It also defines how incision rates will change as the discharge becomes flashier Gasparini and Brandon [2011].

Table 2 contains descriptions of the problem such as the evolution time, the area of the landscape given by its width and length, the amount of time taken to run the Badlands model, and the resolution factor (Res. factor) which indicates the distance in kilometres (km) between two neighbouring points (pts) along x or y-axis of the topography grid. Table 2 give details of the initial conditions used in the simulations for the various problem. Each of these problems features erosion/deposition of sediment over time. Figure 5 shows the change in sediment erosion/deposition at the final stage of evolution

¹ <https://github.com/badlands-model/pyBadlands/tree/master/Examples>

given by the Badlands model. Note that the positive values indicate deposition and the negative values indicate erosion. The yellow dots indicate the locations for the ground-truth data for sediment erosion/deposition history. Hence, the likelihood function given in the following subsection takes both the landscape topography and erosion-deposition ground-truth into account.

Topography	T_{max} (years)	Length [km, pts]	Width [km, pts]	Res. factor	Run-time (s)
Cr	50 000	[0.24, 123]	[0.24, 123]	0.002	2.0
Mt	1 000 000	[80,202]	[40,102]	1.000	10.0
CM	1 000 000	[136.0, 136]	[123.0, 123]	1.000	7.5

Table 1: Landscape evolution problems where the run-time represents the approximate length of time for one sample (simulation by Badlands) to run. The resolution factor (Res. factor) indicates the distance in kilometres (km) between two neighbouring points (pts) along x or y-axis of the topography grid. T_{max} denotes the maximum evolution time in years.

Topography	ρ (m/yr)	k	ν	μ	β	γ	u
Cr	1.5	5.0-e05	1.0	0.5	-	-	-
Mt	1.5	5.0-e06	1.0	0.5	-	-	1.0
CM	1.5	5.0-e06	1.0	0.5	0.5	0.8	-

Table 2: Selected values of parameters used to generate synthetic ground-truth topographies. The parameters include precipitation (ρ) in meters per year (m/yr), erodibility (k), m-value (μ), n-value (ν), marine (β), surface (γ) and uplift (u) in millimeters per year (mm/yr)

3.2 Model and Priors for Parallel Tempering Bayeslands

We assume that topography at time t , and location s_i i.e. $D_{s_i,t}|\boldsymbol{\theta}, \mathbf{D}_0$, has normal distribution with an expected value equal to the Badlands model, given $\boldsymbol{\theta}$ and a variance of τ^2 so that

$$D_{s_i,t} = f_{s_i,t}(\boldsymbol{\theta}) + e_{s_i,t} \text{ with } e_{s_i,t} \sim N(0, \tau^2) \quad (4)$$

for $t = 0, 1, \dots, T$ and $i = 1, \dots, n$; where, n refers to number of observations and T is the maximum simulation time in years. Note that we assume that the observations are independent because the correlation structure of the topography is embedded in the Badlands model.

Although the choice of a normal distribution was made for convenience, we note that there could have been several other choices. For example, we could have assumed that the log of the topography had a normal distribution to allow for negative predicted values which the model given by Equation 4 is capable of producing. We could also assume that the errors were distributed according to a *t-distribution*, or we could model the distribution of errors non-parameterically.

In the model given by Equation 4, we assume an inverse gamma (IG) prior $\tau^2 \sim IG(\nu/2, 2/\nu)$. We integrate it so that the likelihood for the topography at time $t = T$ is $L_t(\boldsymbol{\theta})$ is

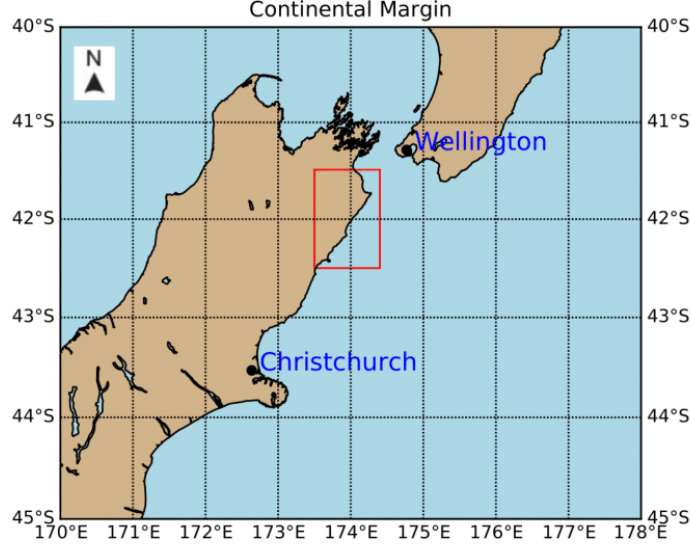


Figure 3: CM problem selected from South Island of New Zealand, outlined by the red rectangle. Note: x-axis represents longitude, while y-axis represents latitude.

$$L_l(\boldsymbol{\theta}) \propto \prod_{i=1}^n \left(1 + \frac{(D_{s_i,T} - f_{s_i,T}(\boldsymbol{\theta}))^2}{\nu} \right)^{-\frac{\nu+1}{2}} \quad (5)$$

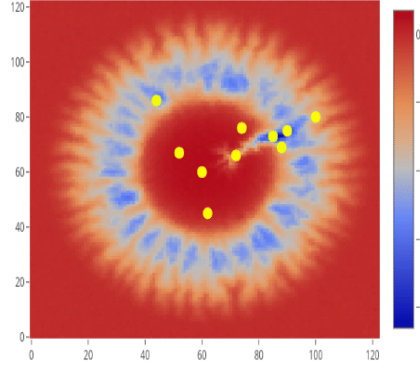
where, the subscript l , in $L_l(\boldsymbol{\theta})$ denotes that it is the landscape likelihood to distinguish it from a sediment likelihood.

Topography	ρ (m/yr)	k	ν	μ	β	γ	λ
Cr	[0, 3.0]	[3.0-e05, 7.0-e05]	[0, 2.0]	[0, 2.0]	-	-	
Mt	[0, 3.0]	[3.0-e06, 7.0-e06]	[0, 2.0]	[0, 2.0]	-	-	[0.1, 5.0]
CM	[0, 3.0]	[3.0-e06, 7.0-e06]	[0, 2.0]	[0, 2.0]	[0.3, 0.7]	[0.6, 1.0]	-

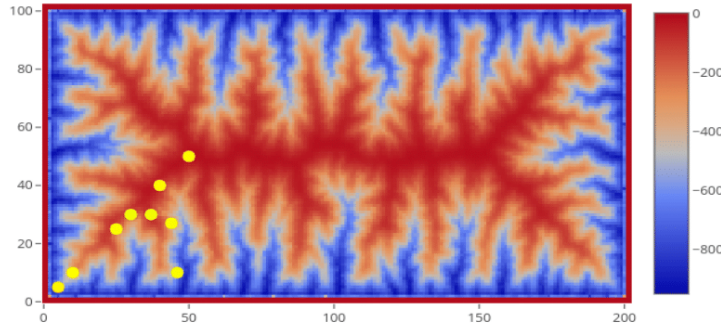
Table 3: Prior distributions of Badlands parameters for precipitation (ρ) in meters per year (m/yr), erodibility (k), m-value (μ), n-value (ν), marine (β), surface (γ) and uplift (λ) in millimeters per year (mm/yr)

As noted in Section 3.1, the history of sedimentary deposits is available at some locations and we use this information to further constrain the number of possible landscape evolution trajectories. Again, we assume that observed sediment erosion/deposition values at time t , \mathbf{z}_t , are a function of the Badlands model, given $\boldsymbol{\theta}$ plus some Gaussian noise

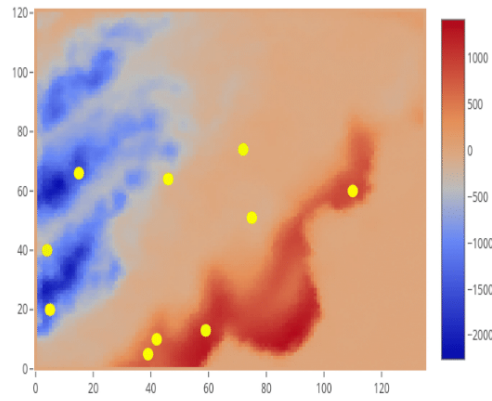
$$z_{s_j,t} = g_{s_j,t}(\boldsymbol{\theta}) + \eta_{s_j,t} \text{ with } \eta_{s_j,t} \sim (0, \chi^2) \quad (6)$$



(a) Cr sediment map



(b) Mt sediment map



(c) CM sediment map

Figure 4: Initial (first column) and final or ground-truth (second column) topographies. Panels (a) and (b) refer to the Synthetic-Crater landscape for $t = 0$ and $t = 50,000$ years respectively. Panels (c) and (d) refer to the Synthetic-Mountain for $t = 0$ and $t = 1,000,000$ years respectively, while Panels (e) and (f) refer to the Continental-Margin landscape for $t = 0$ and $t = 1,000,000$ years respectively.

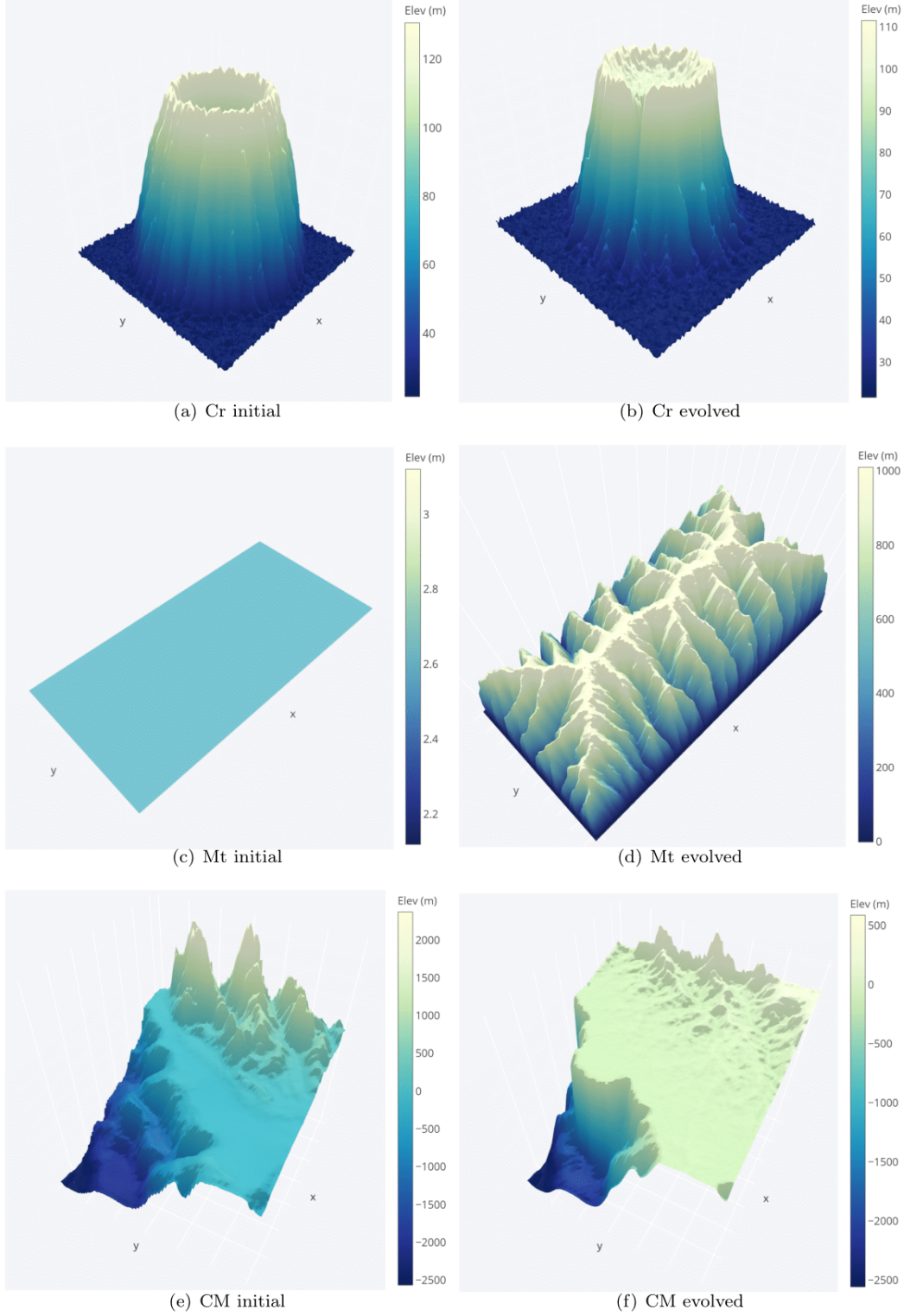


Figure 5: Map view showing evolved model sediment erosion and deposition for each scenario. The selected locations for likelihood evaluation are overlain as yellow dots. The color bars indicate elevation in meters while the x and y axis give the spatial coordinates. Note that positive values indicate deposition and the negative values indicate erosion.

Analogous to the likelihood function for the topography, the sediment likelihood $L_s(\boldsymbol{\theta})$, after integrating out χ^2 is

$$L_s(\boldsymbol{\theta}) \propto \prod_{t=1}^T \prod_{j=1}^J \left(1 + \frac{(z_{s_j,t} - g_{s_j,t}(\boldsymbol{\theta}))^2}{\nu} \right)^{-\frac{\nu+1}{2}} \quad (7)$$

We assume that the elevation observations are independent of the sediment observations, so that

$$L(\boldsymbol{\theta}) = L_s(\boldsymbol{\theta}) \times L_l(\boldsymbol{\theta}) \quad (8)$$

While this assumption may not hold for the simple Cr example, it is not an unreasonable assumption for the CM problem. The complicated topology of the CM problem, together with its coastal location, means that the sediment deposition is dispersed rather than stationary as in the Cr problem.

We use uniform priors for each of the parameters with the lower and upper limits given in Table 3 which reflects on the actual environmental and geological processes. For instance, logically, the values of precipitation and erodibility cannot be below zero. The upper limit is determined by trial experiments and also literature review [Salinger, 1980; Ummenhofer and England, 2007], in order to have realistic assumption for the given problems. For instance, we reviewed the precipitation for South Island in New Zealand over the last few decades and gathered that the upper limit of 3 meters per year (m/a) would be a realistic assumption.

3.3 Sampling Scheme

3.3.1 Within Replica Sampling: proposal distributions

PT-Bayeslands employs a random-walk sampler for each replica which is executed as a separate process. The random-walk proposal distribution, denoted generically by $q(\boldsymbol{\theta}|\boldsymbol{\theta}^c)$ is a multivariate normal distribution with mean vector $\boldsymbol{\mu}$ and covariance matrix Σ . The mean vector $\boldsymbol{\mu}$ is set to the current value in the chain, $\boldsymbol{\theta}^c$. We investigate the use of two different covariance matrices, hereafter known as the standard Random-Walk (SRW) and Adaptive Random-Walk (ARW) proposal distribution.

In the SRW proposal distribution, Σ is fixed to be diagonal, so that $\Sigma = \text{diag}(\sigma_1^2, \dots, \sigma_P^2)$; where σ_j is the step size of the j^{th} element of the parameter vector $\boldsymbol{\theta}$. The step-size for parameter θ_j is chosen to be a combination of a fixed step size ϕ which is common to all parameters, multiplied by the range of possible values for parameter θ_j , so that

$$\sigma_j = (a_j - b_j) \times \phi \quad (9)$$

where, a_j and b_j represent the maximum and minimum limits of the prior for θ_j given in Table 2.

In the ARW proposal distribution, Σ is adapted every M intervals of within-replica sampling. Σ allows for the dependency between elements of $\boldsymbol{\theta}$ and changes throughout the within replica proposals sampler [Haario *et al.*, 2001]. The elements of Σ are adapted to the posterior using the sample covariance of the current chain history: $\Sigma = \text{cov}(\{\boldsymbol{\theta}^{[0]}, \dots, \boldsymbol{\theta}^{[i-1]}\}) + \text{diag}(\lambda_1^2, \dots, \lambda_P^2)$; where $\boldsymbol{\theta}^{[i]}$ is the i^{th} iterate of $\boldsymbol{\theta}$ in the chain and λ_j is the minimum allowed step sizes for each parameter θ_j .

Given the current value $\boldsymbol{\theta}^c$, the proposed value for $\boldsymbol{\theta}$ denoted by $\boldsymbol{\theta}^p$, is accepted with probability α . This with uniform priors and symmetric proposal distribution reduces to;

$$\alpha = \min \left(1, \frac{L(\mathbf{D}_T, \mathbf{Z}|\theta^p)}{L(\mathbf{D}_T, \mathbf{Z}|\theta^c)} \right) \quad (10)$$

3.3.2 Between-Replica Sampling

The *replica transition* procedure considers the exchange of two neighboring replicas. Suppose there are M replicas indexed by m , with corresponding stationary distributions $p_m(\theta|\mathbf{D}_T) = p(\theta|\mathbf{D}_T)^{\beta_m}$; for, $m = 1, \dots, M$, with $\beta_1 = 1$ and $\beta_M < \beta_{M-1} < \dots, \beta_1$ and define the temperature ladder to be $\beta = (\beta_M, \dots, \beta_1)$. The total parameter space consists of the chain m and the parameters within those replicas θ_m and then the pair (m, θ) are jointly proposed and accepted/rejected according to the Metropolis-Hasting (MH) algorithm. The stationary distribution of chain m is $p(\theta_m|\mathbf{D}_t, \mathbf{Z})^{\beta_m}$. Suppose chains m and $m+1$ are at iteration k , with parameter values $\theta_m^{[k]}$ and $\theta_{m+1}^{[k]}$, which we denote as θ_m^c and θ_{m+1}^c ; where, the superscript c represents the current value. We propose a swap between these chains so that $\theta_m^p = \theta_{m+1}^c$ and $\theta_{m+1}^p = \theta_m^c$; where, the superscript p represents the proposed value. We accept the proposed values with probability

$$\alpha = \min \left\{ 1, \left[\frac{p(\theta_m^c|\mathbf{D}_T, \mathbf{Z})}{p(\theta_{m+1}^c|\mathbf{D}_T, \mathbf{Z})} \right]^{(\beta_{m+1} - \beta_m)} \right\} \quad (11)$$

If accepted, $\theta_{m+1}^{[k+1]} = \theta_{m+1}^p$ and $\theta_m^{[k+1]} = \theta_m^p$; otherwise, the chain remains where it is, $\theta_{m+1}^{[k+1]} = \theta_{m+1}^{[k]}$ and $\theta_m^{[k+1]} = \theta_m^{[k]}$. We note that each of the replicas are assigned with a temperature ladder that relaxes the likelihood which affects the MH acceptance probability. Essentially, the replicas with higher temperature values have more probability of within replica proposal acceptance which can help in escaping from sub-optimal modes. Given that the temperature ladder is user-defined, it is dependent upon the nature of the posterior. We use a geometric temperature ladder with

$$\beta_m = 1/\tau_m, \beta_M = 1/M \text{ and therefore, } \beta_m = \beta_{m-1}M^{-1/(M-1)} \quad (12)$$

for $m = 2, \dots, M$ where M is the number of replicas and τ is the maximum temperature which is user defined.

3.4 Multi-core parallel tempering Bayeslands

Bayeslands is comprised of the Badlands forward model embedded in a PT-MCMC sampling scheme, both of which are computationally expensive, and thus the combination of the two presents several challenges. We note that in PT-MCMC, the replica with temperature level of 1 only becomes part of the posterior. The rest of the replicas are used to enhance exploration by escape from local minima. It is via the replica exchange that the configuration from the rest of the replicas become part of the posterior, provided that they move to replica with temperature of 1. It is unfeasible to draw large number of samples given that the Badlands model is computationally expensive and hence the likelihood evaluation adds to the overall cost of sampling. Hence, we need efficient sampling within limited time, given by number of samples drawn.

To address this problem, we split the sampling scheme into two phases. The first phase uses parallel tempering with a temperature ladder as defined by Equation 12. The second phase sets the temperature ladder to be a vector of ones. Essentially, the first phase is used to ensure that the starting values of the second phase cover most of the parameter space. The second phase still exchanges between adjacent chains to avoid them getting stuck in local modes. Figure 6 gives an overview of the different replicas that are executed on a multi-processing architecture. The task of the main process in Figure 6 is to manage the ensemble of replicas which runs on a separate processing core. Given

there are M replicas with each replica running on a separate core, there will be $M+1$ processes in total. The Badlands model is executed in the same processing core as the within replica sampling, and inter-process communication is used to exchange neighboring replicas [Lamport, 1986]. To enhance computational efficiency, we minimize inter-process communication by only allowing replica exchanges at user defined fixed intervals. The main process waits for all replicas to complete sampling until the swap interval is reached in order to attempt replica exchange. Then the main process notifies the replicas to resume sampling with latest configurations in the chain for each replica.

Algorithm 1 outlines the sampling scheme. It first initializes the number of replicas M , the maximum number of iterations, Iter_{\max} , the swap interval Swap_{int} , and the temperature ladder $\beta = (\beta_M, \dots, \beta_1)$ before drawing the initial values of θ_m for $m = 1, \dots, M$ from the prior $p(\theta)$. Then, Algorithm 1 executes each of the replicas in parallel as in Figure 6. Each replica θ is updated when the respective proposal is accepted/rejected using the MH acceptance criterion given by Step 1.4 and the new value of θ is added to the posterior distribution as shown in Step 1.3. This procedure is repeated until the replica swap interval is reached (Swap_{int}) which determines how often the algorithm pauses and checks if neighbouring replicas can be swapped using MH criterion (Step 2.3). The procedure is repeated until the termination condition is satisfied which is given by the maximum number of iterations.

It is generally expected that increasing the number of replicas in PT-Bayeslands will shorten the computation time; however, this is not necessarily true because additional time is taken with inter-process communication. The effect of increasing the number of replicas on the performance accuracy will be investigated.

Alg. 1 Multi-core Parallel Tempering MCMC**Result:** Draw iterations from $p(\theta|\mathbf{D}_T, \mathbf{Z})$

i. Set maximum number of iterations (Iter_{\max}), the swap interval (Swap_{int}), the number of replicas (M), the percentage of iterations for parallel tempering phase and the temperature ladder

$$\beta = (\beta_M, \dots, \beta_1).$$

ii. Initialize replica $\theta_m = \theta_{m^{[0]}}^{[0]}$, for $m = 1, \dots, M$.

iii. Set the current values; $\theta_m^c = \theta_{m^{[0]}}^{[0]}$, and $m^c = m^{[0]}$

```

while  $\text{Iter}_{\max}$  do
  for  $m = 1, \dots, M$  do
    for  $k = 1, \dots, \text{Swap}_{\text{int}}$  do
      *Parallel Tempering Phase
      if tempering is false then
        |  $\beta = 1_M$ 
      end
      *Parallel Tempering Phase
      Step 1: Replica sampling
      1.1 Propose  $\theta^p$ 
      1.2 Compute acceptance probability as in Equation 10
      1.4 Acceptance criterion Draw  $u \sim U[0, 1]$ 
      if  $u < \alpha$  then
        |  $\theta^{[k]} = \theta^p$ 
      else
        |  $\theta^{[k]} = \theta^c$ 
      end
    end
    Step 2: Replica Exchange
    2.1 Propose replica swap .
    2.2 Compute acceptance probability as given by Equation 11
    2.3 Acceptance criterion
    Draw  $u \sim U[0, 1]$ 
    if  $u < \alpha$  then
      |  $\theta_m^{[k]} = \theta_{m^p}^p$ 
    else
      |  $\theta_m^{[k]} = \theta_{m^c}^c$ 
    end
  end
end

```

3.5 Evaluation

The performance of PT-Bayelands is evaluated in three ways. The first is by comparing the posterior distributions of the parameters with those used to generation the data. The second is by comparing the computational time for the PT-Bayeslands versus single chain MCMC (SC-Bayeslands) from earlier work [Chandra *et al.*, 2019b]. The third is by comparing the predicted/simulated Badlands landscape with the ground-truth data using the root-mean squared error (RMSE). The RMSE for the elevation (elev) and sediment erosion/deposition (sed) is computed at each iteration of the sampling scheme and are given by

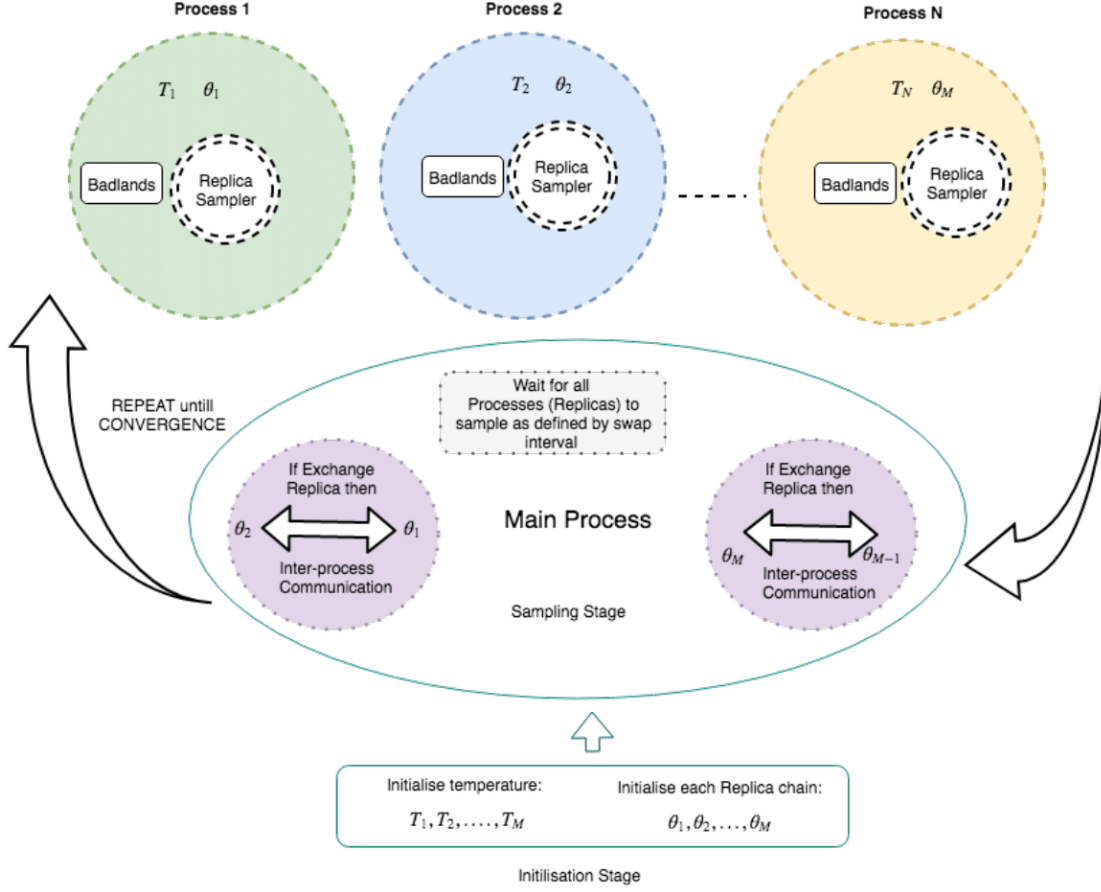


Figure 6: An overview of the different replicas that are executed on a multi-processing architecture for PT-Bayeslands. Note that the main process controls the given replicas and enables them to exchange the neighboring replicas.

$$\text{RMSE}_{elev} = \sqrt{\frac{1}{n \times m} \sum_{i=1}^n \sum_{j=1}^m \left(g(\hat{\theta}_{T,i,j}) - g_{T,i,j}(\theta) \right)^2}$$

$$\text{RMSE}_{sed} = \sqrt{\frac{1}{n_t \times v} \sum_{t=1}^{n_t} \sum_{j=1}^m \left(f(\hat{\theta}_{t,j}) - f(\theta_{t,j}) \right)^2}$$

where, $\hat{\theta}$ is an estimated value of θ , chosen according to the proposal distribution and θ is the true value on which the ground truth topographies and sediment thickness were based. $f(\cdot)$ and $g(\cdot)$ represent the outputs of the Badlands model, as defined earlier while m and n represent the size of the selected topography. v is the total number of selected points from sediment erosion/deposition as shown in Figure 5 over the selected time frame, n_t . Apart from the three application problems (Cr, Mt, CM), we also test the performance of PT-Bayeslands to the different user settings, such as exchange rate Swap_{int} , and the maximum number of iterations Iter_{max} .

4 Results

4.1 Estimated Topography Elevation and Sediment Erosion/Deposition

We show the estimates of the posterior mean elevation and the sedimentary erosion/depositions produced by PT-Bayeslands for all three landscape problems and compare these with the ground-truth. For all three problems, the number of iterations was fixed at 10,000 with 10 replicas, and a SRW was used as a proposal distribution. PT-Bayeslands produces posterior means of the elevation and sedimentary deposits each year but due to limited space, we show these figures for only two selected years; one half way through the evolution and the other at the end of the evolution.

Figure 7 shows the elevation of the Cr problem after 25,000 and 50,000 years. Figures 8 and 9, are analogous plots for the CM and Mt problems for 500,000 years and 1,000,000 years, respectively. These plots show how well PT-Bayeslands estimates the final elevation ground truth.

Figures 10, 11 and 12 show the sedimentary erosion/deposition at the same two selected time slices. These sedimentary erosion/deposition data were taken at 10 selected points across the given landscape (Figure 5). The posterior mean is shown in black while the ground truth is shown in green. These figures show how well PT-Bayeslands approximates the sedimentary erosion/disposition when compared to the ground truth at selected times.

4.2 Multi-modality

Geophysical inversion problems often exhibit parameter posterior distributions which are multi-modal. Figure 13 shows the log posterior for precipitation and uplift while fixing all other parameters in the Mt problem. We again note that our previous work [Chandra *et al.*, 2019b] showed that different combinations of precipitation and erodibility gave rise to visually indistinguishable topography for both the Cr and CM problem.

Figure 13 shows that the posterior has a ridge-like structure which is similar to Figure 1; however, the surface exhibits so many discontinuities that resemble CM posterior surface in Figure 2. We found that SC-Bayeslands had difficulty to uncover or efficiently sample the structure. In this case, even PT-Bayeslands will face difficulties and carefully crafted proposal distribution and temperature ladder will be required to efficiently explore the space.

4.3 Performance comparison for simpler problems

To further investigate the issue of multi-modality, we compared PT-Bayeslands with SC-Bayeslands for the respective problems in different settings. In the first setting, we allowed only one parameter at a time to vary and fixed the other parameters to their true value. The parameters that were allowed to vary were precipitation (ρ) and erodibility k for the Cr and CM problem while rest were fixed to true values shown in Table 2. In the second setting, ρ and k were allowed to vary simultaneously while fixing the remaining parameters.

Figure 14 shows histogram estimates of the posterior distribution for ρ , and trace plots of the iterates of ρ from PT-Bayeslands for the Cr problem, while fixing all the other parameters. The true value of ρ is 1.5 m/a which is given by the vertical red line that appears in the centre of the distribution. The trace plot shows that the replicas mix well. Similar plots for the other parameters and on the CM problem were also obtained.

Figure 15 displays results for the Cr problem in the second setting. Figure 15, Panels (a) and (c.) show histogram estimates of the posterior distribution of ρ , when both ρ and k are allowed to vary. Panel (a) displays the estimated histogram using SC-Bayeslands,

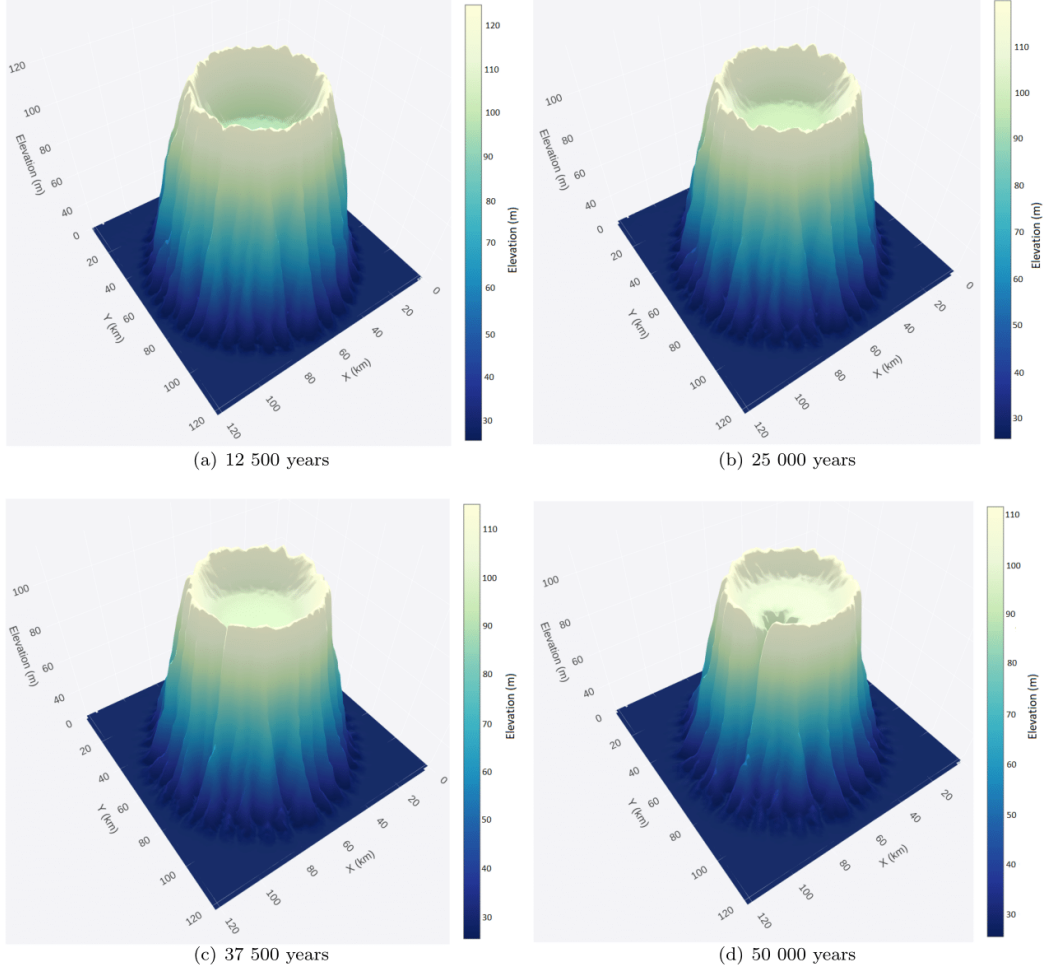


Figure 7: Badlands landscape evolution for 4 different time-scales for the Synthetic-Crater showing the elevation topography, for 10 000 iterates with 10 replicas, using simple random-walk as a proposal distribution from results shown in Table 8.

while panel (c) displays the estimated histogram using PT-Bayeslands. Panels (b) and (d) are the corresponding trace plots. These plots show how PT-Bayeslands vastly improves the exploration of the parameter space. The sampler in SC-Bayeslands explores one mode for the first 20,000 iterations and then appears to shift to another mode for the remaining iterations. In contrast, PT-Bayeslands explores the values of ρ corresponding to the entire ridge in Figure 1.

Figure 16 displays results for the CM problem which shows a similar trend. Although PT-Bayeslands performs better than SC-Bayeslands (Figure 16), the mixing between chains is still poor. This is due to the large number of local modes in the log-posterior surface shown in Figure 2, which earlier highlighted the challenges of sampling. Figure 2 shows that the number of modes is much greater than the number of chains, and a possible solution to this is to add more chains, but then the sampler is not computationally feasible.

Table 4 shows the results from the experiments for the different combination of parameters for the two methods. Note that the total prediction accuracy is given for model

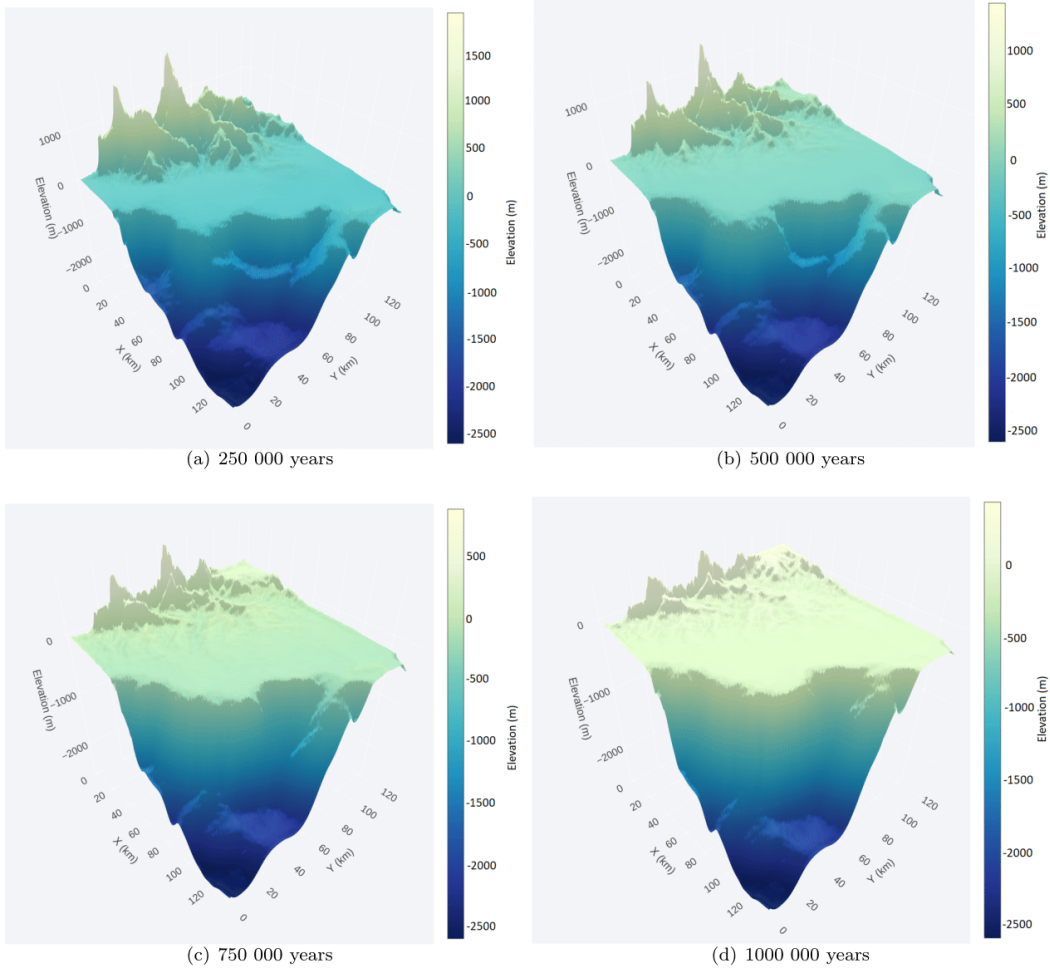


Figure 8: Badlands landscape evolution for 4 different time-scales for the Continental-Margin showing the elevation topography for 10000 iterates with 10 replicas, using simple random-walk as a proposal distribution from results shown in Table 8.

elevation topography and sedimentary thickness in terms of accuracy given as posterior mean of $\text{RMSE}_{\text{elev}}$ and RMSE_{sed} . The sediment RMSE considers the ground-truth and final sediment distribution averaged over selected points in the model domain (see Figure 5). The results show that both methods achieve equally consistent prediction accuracy. However, PT-Bayeslands significantly reduces the computational time taken while also having better exploration features as shown in Figure 15.

4.4 Effect of simulation setting

In this section, the effect of the number of replicas, the number of iterations, and the swap rate are evaluated using the CM problem given all six free parameters as shown in Table 3. This problem was selected for these experiments because it has a difficult log-posterior surface with a single optimal mode and many sub-optimal modes. Table 5 provides metrics for each of the settings, where each setting has a total number of 10,000 iterations. For example, the first setting has 10000 iterations spread across 4 chains, therefore a total of 2500 for each while, while last setting has 48 chains and therefore only 208

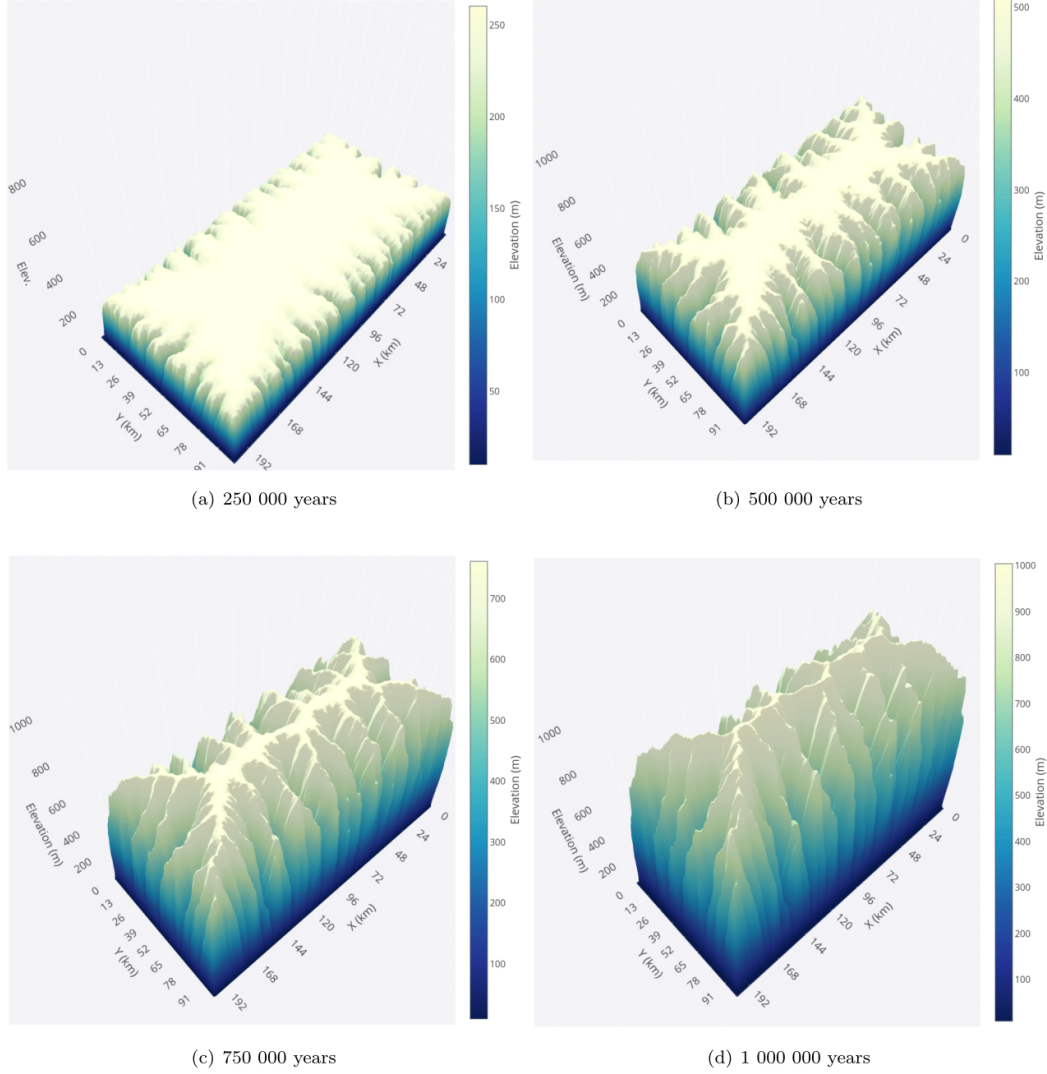


Figure 9: Badlands landscape evolution for 4 different time-scales for the Synthetic-Mountain showing the elevation topography for 10 000 iterates with 10 replicas, using simple random-walk as a proposal distribution from results shown in Table 8.

iterations in each chain. We observe that increasing the number of replicas reduces the overall computation time. However, the number of replicas does not appear to have much effect on the elevation and sediment erosion/deposition prediction accuracy as measured by the $\text{RMSE}_{\text{elev}}$ and RMSE_{sed} .

We then evaluate the effect that an increase in the number of iterations has on the prediction accuracy of PT-Bayeslands, for a given number of replicas. Table 6 presents summary of the results for the CM topography with 10 replicas. Obviously, increasing the number of iterations increases the overall time taken in a linear fashion. The relationship between the number of iterations and the prediction accuracy is non-linear given diminishing improvements to prediction accuracy as the number of iterations is increased. The optimal setting depends upon the trade-off between computational speed and prediction accuracy. We find that the interval 20,000 to 50,000 iterations is reasonable.

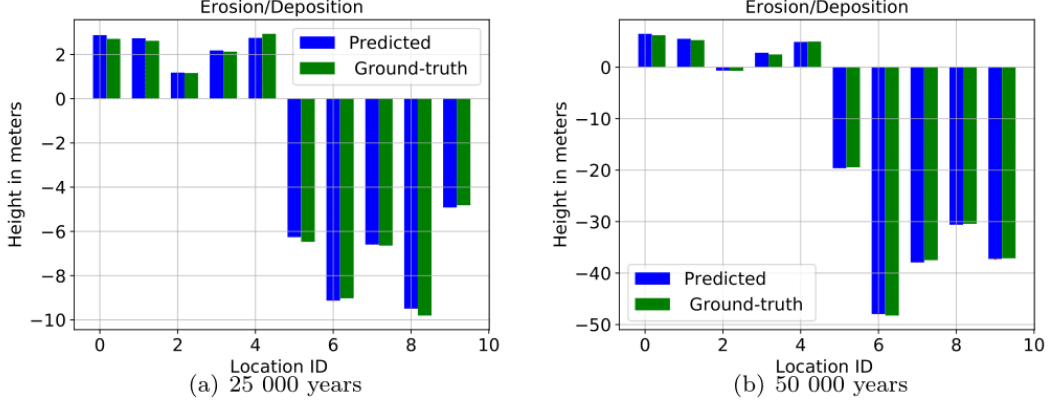


Figure 10: Badlands landscape evolution for 2 selected time-scales corresponding to Figure 7 for the Synthetic-Crater showing the sedimentary deposition for 10 selected points.

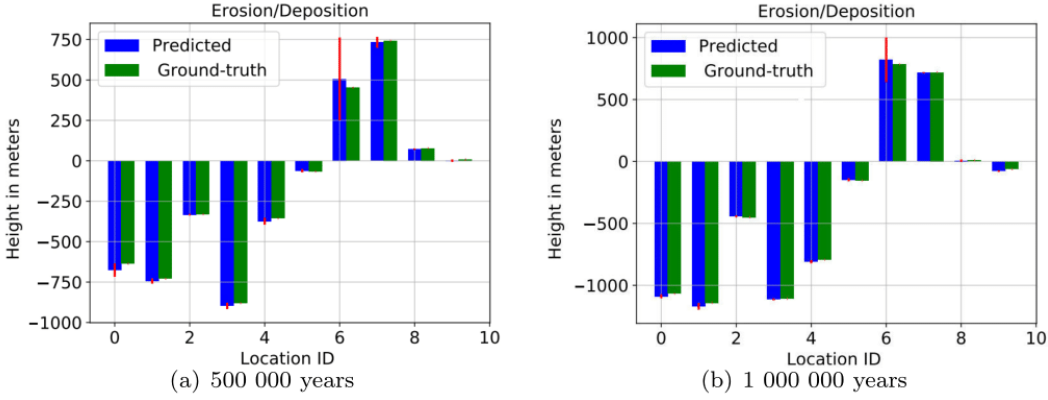


Figure 11: Badlands landscape evolution for 2 selected time-scales corresponding to Figure 8 for the Continental-Margin showing the sedimentary deposition for 10 selected points. The red lines show the uncertainty in prediction given by 95 % credible interval.

Table 7 contains the results of an experiment to investigate the effect of the replica exchange rate (Swap-Rate) on the prediction accuracy and the percentage of swaps accepted for the CM problem. Here, we used 10,000 iterations with 10 replicas. The results show that the Swap-Rate has a negligible effect on the prediction accuracy.

4.5 Effect of the Proposal Distribution

In this section, we allow the number of iterations and the number of replicas to jointly vary, as well as allowing the proposal distribution (SRW and ARW). The effect of these different settings on the prediction accuracy is evaluated for all three landscape problems shown in Table 8. A major observation in Table 8 is that the proposal distribution does not effect the prediction accuracy.

Table 9 shows convergence results for the two different proposal distributions as measured by the Gelman-Rubin diagnostic [Gelman *et al.*, 1992]. The Gelman-Rubin diagnostic evaluates MCMC convergence by analyzing the behaviour of multiple Markov chains. Given multiple chains from different experimental runs, assessment is done by

Problem	Method	Parameters allowed to vary	Time (minutes)	$RMSE_{elev}$ pos. mean	$RMSE_{sed}$ pos. mean
Synthetic-Crater	SC-Bayeslands	ρ	355.92	1.040	0.179
	SC-Bayeslands	k	356.18	1.05	0.180
	SC-Bayeslands	ρ, k	355.39	1.05	0.170
	PT-Bayeslands	ρ	44.05	1.050	0.180
	PT-Bayeslands	k	42.31	1.050	0.180
	PT-Bayeslands	ρ, k	39.91	1.050	0.180
Continental-Margin	SC-Bayeslands	ρ	418.0	52.4	34.1
	SC-Bayeslands	k	423.70	51.50	43.30
	SC-Bayeslands	ρ, k	415.80	44.00	48.90
	PT-Bayeslands	ρ	59.40	58.3	48.10
	PT-Bayeslands	k	64.70	59.6	46.90
	PT-Bayeslands	ρ, k	60.60	60.3	50.60

Table 4: Comparison of SC-Bayeslands and PT-Bayeslands for the CM and Cr problems. The parameter column presents the parameters that are estimated while keeping other model parameters fixed to their true values. The time taken for SC-Bayeslands and PT-Bayeslands is reported along with the accuracy given as posterior mean (pos. mean) of $RMSE_{elev}$ and $RMSE_{sed}$.

Replicas (cores)	Time (minutes)	$RMSE_{elev}$ (pos. mean)	$RMSE_{sed}$ (pos. mean)
4	153.2	58.6	43.3
8	80.5	56.9	48.7
10	63.4	60.4	49.1
12	60.0	56.7	47.9
16	43.4	67.2	52.3
20	35.3	67.6	52.8
24	30.2	68.6	51.2
30	26.1	69.0	51.5
36	22.7	71.7	53.7
42	20.1	71.1	53.0
48	19.1	75.7	52.9

Table 5: Effect of increasing the number replicas for the CM topography with 10 000 total iterations. The prediction accuracy is given as posterior mean (pos.mean) of $RMSE_{elev}$ and $RMSE_{sed}$.

iterations	Time (minutes)	$RMSE_{elev}$ (pos. mean)	$RMSE_{sed}$ (pos. mean)
1000	6.5	80.6	64.1
5000	29.4	67.5	49.4
10000	54.1	61.5	52.8
20000	130.5	57.3	51.2
50000	279.3	49.0	45.7
100000	518.3	48.6	43.2

Table 6: Effect of the number of iterations for the CM problem with 10 replicas. The prediction accuracy is given as posterior mean (pos.mean) of elevation $RMSE_{elev}$ and sediment $RMSE_{sed}$.

Swap-Rate	Time (minutes)	RMSE _{elev} (pos. mean)	RMSE _{sed} (pos. mean)	Swap %
0.01	88.4	69.9	51.2	22.2
0.02	94.6	72.8	58.6	23.0
0.03	100.2	76.7	58.2	21.8
0.04	91.5	66.1	46.5	22.4
0.05	90.1	63.9	45.2	22.9
0.06	94.5	74.5	51.9	23.4
0.07	90.1	69.7	50.7	22.0
0.08	92.5	71.1	51.7	22.2
0.09	88.5	67.5	44.3	25.7
0.10	95.2	69.8	58.2	22.8

Table 7: Effect of the swap-rate for the CM problem with 10 replicas (10, 000 iterations in total). Note that the posterior mean (pos. mean) for accuracy in terms of RMSE_{elev} and RMSE_{sed} are given in meters. The percentage swap (Swap %) gives an indication of number of proposals that were successfully exchanged. The prediction accuracy is given as posterior mean (pos. mean) of elevation RMSE_{elev} and sediment RMSE_{sed}.

Topography	Parameters	Proposals	Replica	T_{max}	RMSE _{elev} (mean, std)	RMSE _{sed} (mean, std)	Swap%
Cr	4	SRW	10	10 000	(1.05, 0.01)	(0.18, 0.01)	22.15
			20	50 000	(1.05, 0.01)	(0.18, 0.01)	13.09
		ARW	10	10 000	(1.05, 0.01)	(0.18, 0.01)	33.66
			20	50 000	(1.05, 0.01)	(0.18, 0.01)	26.33
Mt	5	SRW	10	10 000	(6.30, 3.11)	(0.87, 1.18)	22.31
			20	50 000	(5.48, 1.36)	(0.54, 0.51)	13.26
		ARW	10	10 000	(6.69, 2.55)	(0.69, 0.60)	22.30
			20	50 000	(5.44, 1.72)	(0.48, 0.37)	13.26
CM	6	SRW	10	10 000	(61.68, 17.31)	(45.74, 25.31)	23.62
			20	50 000	(61.86, 8.64)	(48.38, 17.97)	14.32
		ARW	10	50 000	(70.56, 8.38)	(50.80, 12.50)	31.87
			10	50 000	(63.02, 11.48)	(52.53, 20.81)	27.22

Table 8: Typical results in PT-Bayeslands using simple random-walk (SRW) and adaptive random-walk (ARW) proposal distributions for the three problems (Cr, Mt and CM). T_{max} denotes the maximum number of iterations and the mean and standard deviation (std) of topography elevation (RMSE_{elev}) and sediment erosion/deposition (RMSE_{sed}) prediction accuracy is shown.

Topography	Proposal	ρ	k	γ	λ	β	ϕ	u
Cr	SRW	4.71	5.19	2.63	11.49	-	-	-
	ARW	4.39	3.79	1.25	1.13	-	-	-
Mt	SRW	5.99	8.57	10.29	13.62	12.55	7.27	-
	ARW	1.78	1.77	1.17	1.33	1.12	1.24	-
CM	SRW	4.48	3.11	2.63	6.14	-	-	2.81
	ARW	1.73	1.89	1.16	1.34	-	-	1.21

Table 9: Convergence diagnosis showing the potential scale reduction factor (PSRF) score for the simple random-walk (SRW) and adaptive random-walk (ARW) proposal distributions for the three problems (Cr, Mt and CM) are shown. The respective parameters include; precipitation (ρ), erodibility (k), m-value (γ), n-value (λ), marine (β), surface (ϕ) and uplift (u).

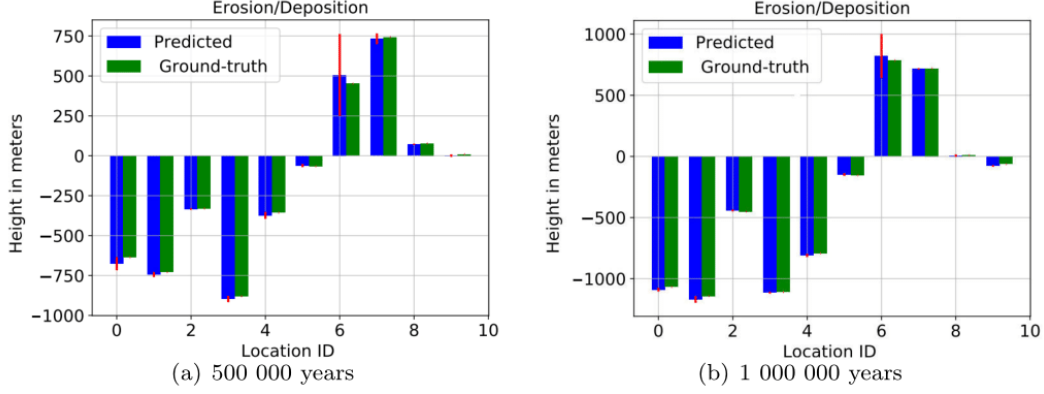


Figure 12: Badlands landscape evolution for 2 selected time-scales corresponding to Figure 9 for the Synthetic-Mountain showing the sedimentary deposition for 10 selected points. The red lines show the uncertainty in prediction given by 95 % credible interval.

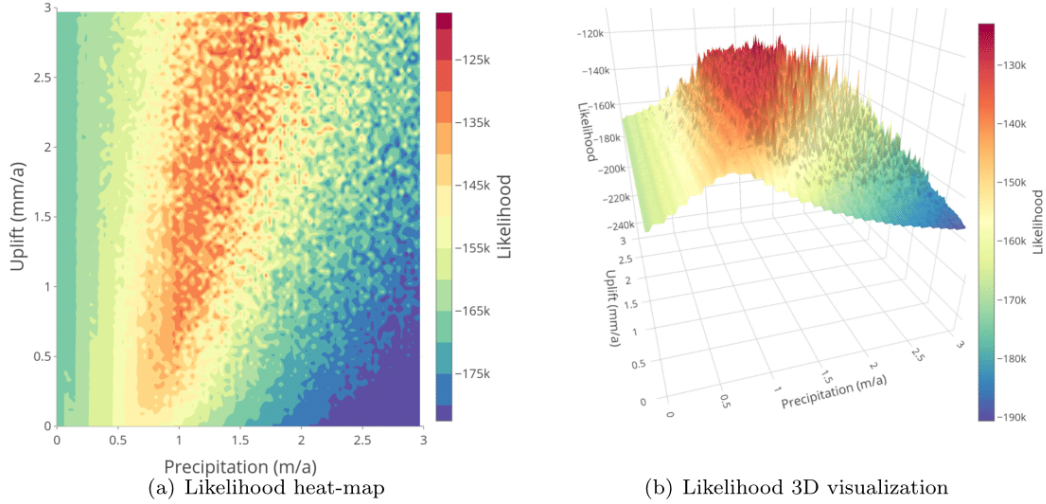


Figure 13: Panels (a) and (b) are a heat map and a surface plot of the log posterior surface of the Mountain problem as function of precipitation, ρ , and erodibility, k .

comparing the estimated between-chains and within-chain variances for each parameter, where large differences between the variances indicate non-convergence. We provide convergence diagnosis for the two different proposal distributions (SRW and ARW) by running multiple chains using different initial values for 10,000 iterations for each topography problem. We calculate the potential scale reduction factor (PSRF) which gives the ratio of the current variance in the posterior variance for each parameter compared to that being sampled. The values for the PSRF near 1 indicates convergence. Table 9 shows that the ARW proposals in general provide much better convergence when compared to SRW proposals. The only case where ARW is not near 1 is for two parameters (ρ , k).

Figure 17 show the posterior mean and associated uncertainty of a cross section through the Y axis, with the X axis held constant at its middle value for both the SRW

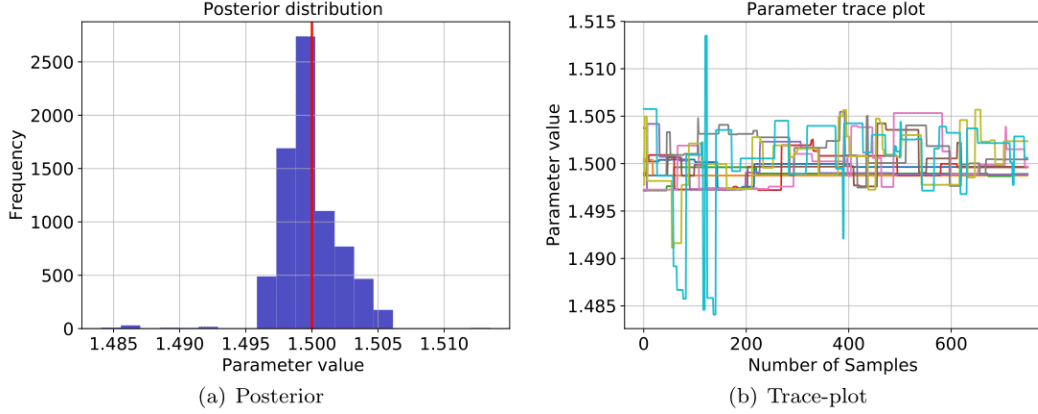


Figure 14: PT-Bayeslands for Cr problem with one parameter (precipitation) for 10, 000 iterations. The panels show estimates of the posterior distribution and trace-plot of the precipitation (ρ). The trace-plots show the accepted or current values of the chain for the given samples. The true value is given by red vertical line (1.5 m/yr) in Panel (a).

proposal and the ARW proposal for all the three problems. The figure shows that the estimated cross sectional elevation is visually identical for both types of proposals, as expected theoretically. We note that the uncertainty for the Mt problem is slightly less for the ARW than the SRW, suggesting that the SRW may not have converged as quickly.

We present further details for selected parameters for the given problems. We show details of the precipitation posterior for Cr and CM problems. We then show the Mt model uplift posterior as this is a unique parameter not present in the other problems. Figures 18, 20 and 19 show the posterior distribution and trace-plot for selected parameters for the respective problems. Note that the most extensive parameter space exploration by PT-Bayeslands occurs for the Cr problem. The exploration ability of the replicas is visible, given the trace-plot in Figure 18. This is in contrast with the exploration shown in trace-plot given in Mt and CM problems (20 and 19), since they have a highly irregular log-likelihood surface which has a number of sub-optimal peaks. The trace-plot shows that the replicas are essentially trapped in these sub-optimal peaks; increasing the number of replicas (from 10 to 20) and sampling time (from 10,000 to 50 0,000), shows no major difference. However, even these sub-optimal peaks give an acceptable prediction as shown in Figure 17.

In this section, we only presented selected details of the posterior distribution, successive topography, and successive erosion-deposition predictions. Detailed results for all problems are provided in supplementary material online ².

5 Discussion

The results presented in the previous section can be summarised as follows;

1. For multi-modal problems PT-Bayeslands provides better exploration of the posterior than SC-Bayeslands. This improvement in performance is particularly vis-

² Supplementary results: https://github.com/badlands-model/paralleltemp_Bayeslands/tree/master/supplementary_results

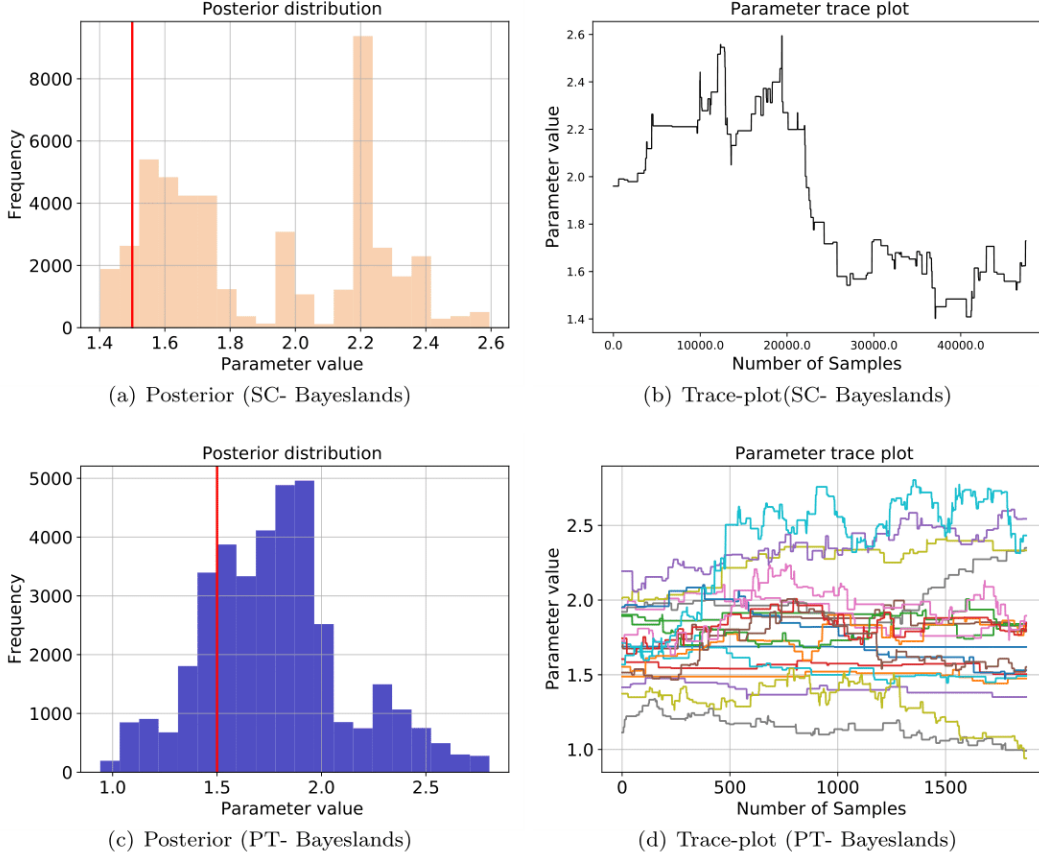


Figure 15: Comparison of PT-Bayeslands with SC-Bayeslands for the Cr problem for 50,000 iterations. The panels show estimates of the posterior distribution and trace-plot of the precipitation (ρ) for the SC-Bayeslands and PT-Bayeslands respectively. The trace-plots show the accepted or current values of the chain for the given samples. Note that the results for SC-Bayeslands are taken from [Chandra *et al.*, 2019b] (with 5 % burnin) while PT-Bayeslands features 25 %burn-in.

- ible when the modes are not connected (as in the CM Mt problem) and as the dimension of the problem increases. Despite the variability in results between SC-Bayeslands and PT-Bayeslands, the predictive performance for both methods is similar. This suggests that SC-Bayeslands has the ability to converge in a sub-optimal mode, even if it does not explore the multi-modal posterior fully. These are important results because multi-modal posterior distributions are typically present in geological and geophysical inversion problems [Dalla Mura *et al.*, 2015; Beskos *et al.*, 2017]. We observed that different experimental runs, depending on initial conditions (starting value), only certain combination of the modes can be recovered.
2. Sampling multimodal distribution is a challenge; however, our results show that convergence on sub-optimal modes gives similar topography evolution when compared with true values. The use of better proposal distributions can help in future work, such as using gradient-free meta-heuristics from field of evolutionary algorithms [Drugan and Thierens, 2003; Ter Braak, 2006]. Moreover, we also need

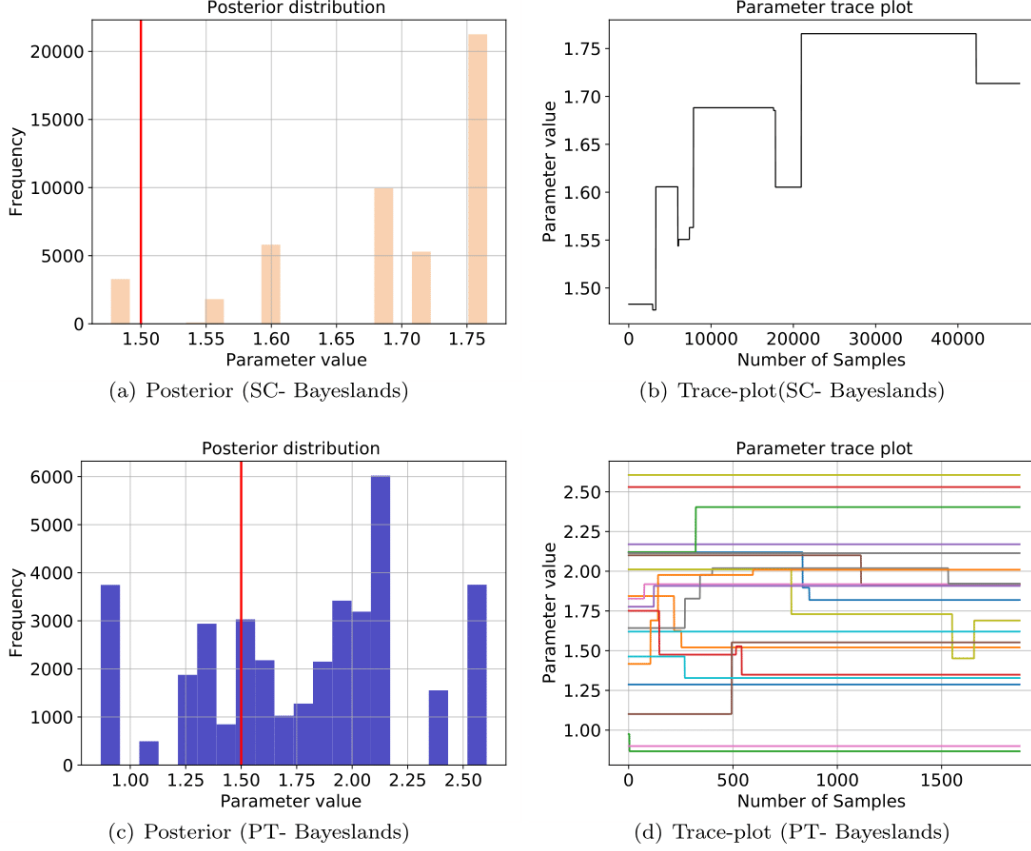


Figure 16: Comparison of PT-Bayeslands with SC-Bayeslands for the CM problem for 50,000 iterations. The panels show estimates of the posterior distribution and trace-plot of the precipitation (ρ) for the SC-Bayeslands and PT-Bayeslands respectively. The trace-plots show the accepted or current values of the chain for the given samples. Note that the results for SC-Bayeslands is taken from [Chandra *et al.*, 2019b] (with 5 % burnin) while PT-Bayeslands features 25 %burn-in.

to incorporate additional data or model constraints that could better help reduce the flexibility of the solution.

3. The computation time for a given number of iterations does not scale linearly with the number of replicas. There is a trade-off between proposing to swap chains and the rate of convergence of the PT-Bayeslands. Swapping proposals between neighboring replicas gives better mixing but introduces computational overhead in a parallel computing environment since each replica needs to wait for all to complete sampling until their swap-interval in order to compute the neighbor swap probability by the managing process. This computational overhead can be higher if the number of replicas is large. We note that the synthetic problems considered in this paper, only required a few seconds of simulation time for Badlands, whereas, in real-world problems, each simulation of Badlands could take several minutes to hours. In such cases, the trade-off between the frequency of swapping and prediction accuracy would need to be evaluated.
4. Increasing the number of cores does not necessarily mean that the prediction accuracy will get better. In particular, it is advantageous to use a larger number of

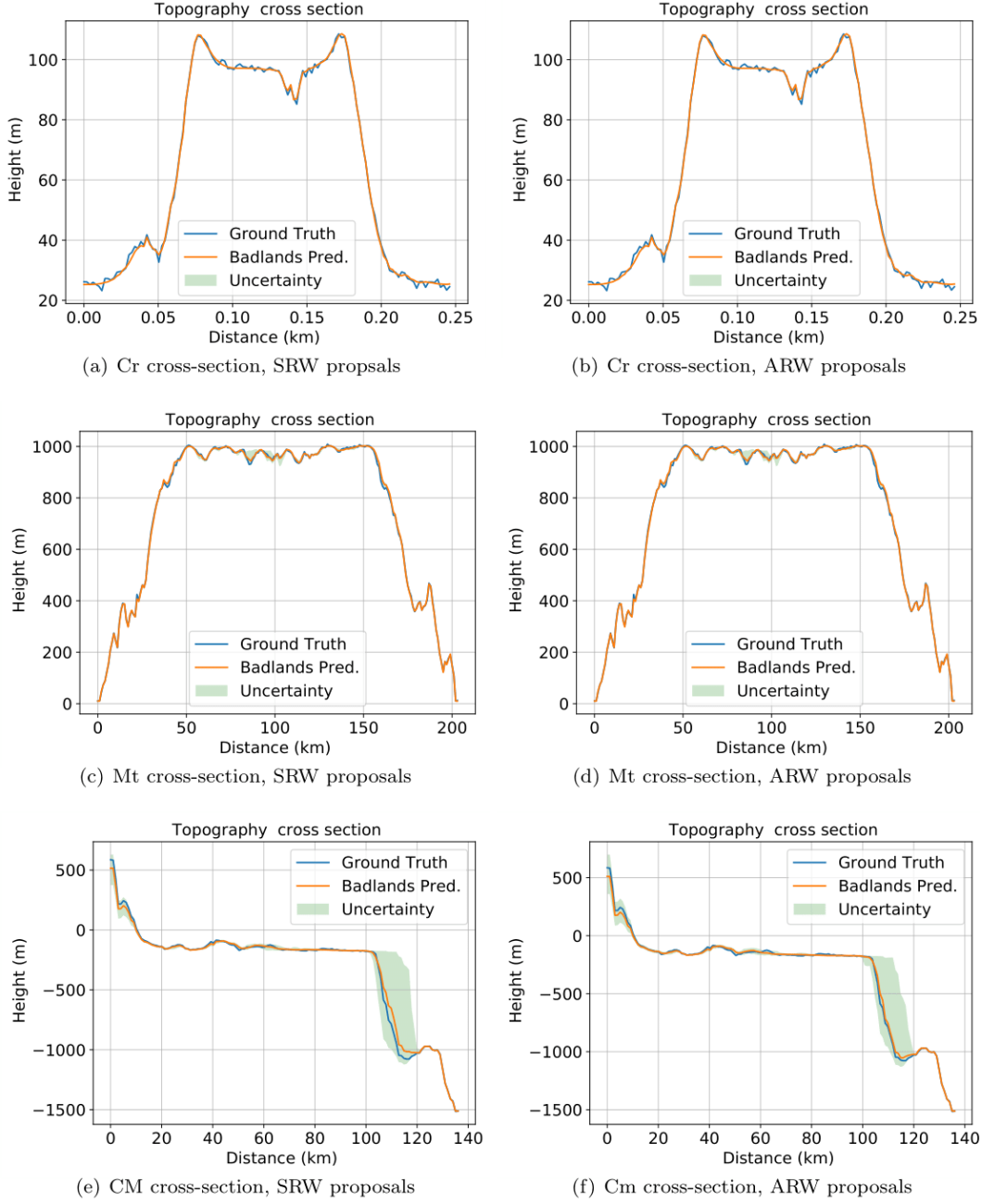


Figure 17: Cross-section comparing the ground-truth evolved topography of the Badlands model with the PT-Bayeslands predictions for the respective problems using SRW and ARW proposal. Note that the x-axis for the subplots are different due to the dimensions of the respective problems.

- cores for large scale problems where the Badlands model takes hours to evaluate a single proposal.
5. The ARW and SRW proposal distributions have the same predictive accuracy; however, the ARW within chain proposal distribution explores the posterior better than the SRW proposal which is evident by the convergence diagnosis shown (Table 9).

6. We highlight that a major limitation in the experiments is the assumption that initial topographies (paleo-elevation) is easily available. We simulated the initial topography and demonstrated the framework with small-scale synthetic problems. We need to note that initial topography is difficult to obtain given limited observations and hence it is a challenge to reconstruct initial topography. The estimation of topography regions which data is not available can be tackled by Bayeslands in future work. The framework can be used to fuse multiple sources of information about initial topography which includes, expert knowledge, data and models for paleo-elevation.
7. The issue of multimodality can be understood by the interpretation of the different factors that affect the topography development over time. Further work could also consider innovative ways to capture these processes in the likelihood function, such as paleo ground-truth data about ancient streams and rivers. Such data can help further constrain the sampling and address problems that arise from multimodality.
8. In Badlands, similar to the model from [Croissant and Braun, 2014], we compute the erosion using a stream power law that links the erosion rate to both the erodibility coefficient of soil, the drainage area and the slope. In future work, the Bayeslands framework could consider other related models. However, changes to the landscape evolution model would feature additional parameters and could have a slightly different likelihood function in order to incorporate the streams and drainage rate that would affect sedimentary deposits.

6 Conclusions and Future Work

The PT-Bayeslands framework provides a rigorous approach for estimation and uncertainty quantification of free parameters in Badlands landscape evolution model using multi-core parallel tempering. We provide a comprehensive experimental evaluation of the method given different combinations of user settings that include sampling time, number of replicas, swap-rate for different types of problems. We also provided a comparison of two different proposal distributions with convergence diagnosis. In general, the results show that the method not only reduces the computation time, but also provides a means to explore the parameter space in highly irregular multi-modal distributions. This has been demonstrated by the results that show better posterior distributions of the parameters along with improvement in prediction accuracy of topography and sediment deposition.

There are several areas of future work. The first is the impact of the temperature ladder on convergence of the MCMC scheme for geophysical inversion problems, see for example [Patriksson and van der Spoel, 2008]. The second is to allow for some parameters, such as precipitation, to vary across space and time. Such a model would allow us to measure the impact of climate change on the environment in terms of sediment erosion/deposition and elevation. We further note that the proposed framework is general and hence, apart from Badlands, it can accommodate other landscape evolution models [Coulthard, 2001] such as the Landlab model [Hobley *et al.*, 2017].

The approach outlined here could be extended by surrogate-assisted models where a surrogate of Badlands would be implemented via machine learning, evaluating the proposals in a fraction of the time taken by actual Badlands runs. This would be of interest for landscape and basin evolution models over long geological time intervals (100 million years and longer) at high resolution whose run time would be prohibitive for a PT-Bayeslands application as outlined here. Further, efficient gradient free proposals would need to be constructed as the number of parameters and the complexity of the model increases.

Acknowledgments

We acknowledge the Strategic Research Excellence Initiative (SREI) Grant from the University of Sydney. Furthermore, we acknowledge the Artemis high performance computing infrastructure provided by Sydney Informatics Hub of the University of Sydney. This work was supported by Australian Research Council grant IH130200012. We sincerely thank Dr. Richard Scalzo for valuable discussions and Ashray Aman for technical support. Furthermore, we would like to sincerely thank the anonymous reviewers and the handling editor for helping us improve the paper.

Data and supplementary material

The selected landscape evolution problems been adapted from examples of the Badlands model ³. Additional results with open software Python code and data is available online ⁴. Supplementary results for the respective problems is also provided online ⁵.

Appendix

Boxplot showing the posterior distribution of the free parameters for the respective problems (Figure 21). The residuals for each topography is shown in Figure 22.

References

- Adams, J. M., N. M. Gasparini, D. E. J. Hobley, G. E. Tucker, E. W. H. Hutton, S. S. Nudurupati, and E. Istanbuluoglu (2017), The landlab v1.0 overlandflow component: a python tool for computing shallow-water flow across watersheds, *Geoscientific Model Development*, 10(4), 1645–1663.
- Beskos, A., M. Girolami, S. Lan, P. E. Farrell, and A. M. Stuart (2017), Geometric mcmc for infinite-dimensional inverse problems, *Journal of Computational Physics*, 335, 327–351.
- Campforts, B., W. Schwanghart, and G. Govers (2017), Accurate simulation of transient landscape evolution by eliminating numerical diffusion: the ttlem 1.0 model, *Earth Surface Dynamics*, 5(1), 47–66.
- Chandra, R., K. Jain, R. V. Deo, and S. Cripps (2019a), Langevin-gradient parallel tempering for bayesian neural learning, *Neurocomputing*, doi:https://doi.org/10.1016/j.neucom.2019.05.082.
- Chandra, R., D. Azam, R. D. Müller, T. Salles, and S. Cripps (2019b), Bayeslands: A bayesian inference approach for parameter uncertainty quantification in badlands, *Computers & Geosciences*, doi:https://doi.org/10.1016/j.cageo.2019.06.012.
- Chen, A., J. Darbon, and J.-M. Morel (2014), Landscape evolution models: a review of their fundamental equations., *Geomorphology*, 219, 68–86.
- Chib, S., and E. Greenberg (1995), Understanding the metropolis-hastings algorithm, *The american statistician*, 49(4), 327–335.
- Coulthard, T. J. (2001), Landscape evolution models: a software review, *Hydrological processes*, 15(1), 165–173.
- Croissant, T., and J. Braun (2014), Constraining the stream power law: a novel approach combining a landscape evolution model and an inversion method., *Earth surface dynamics*., 2(1), 155–166.

³ <https://github.com/badlands-model/pyBadlands/tree/master/Examples>

⁴ <https://github.com/intelligentEarth/pt-Bayeslands>

⁵ https://github.com/badlands-model/paralleltemp_Bayeslands/tree/master/supplementary_results

- Dalla Mura, M., S. Prasad, F. Pacifici, P. Gamba, J. Chanussot, and J. A. Benediktsson (2015), Challenges and opportunities of multimodality and data fusion in remote sensing, *Proceedings of the IEEE*, 103(9), 1585–1601.
- Drugan, M. M., and D. Thierens (2003), Evolutionary markov chain monte carlo, in *International Conference on Artificial Evolution (Evolution Artificielle)*, pp. 63–76, Springer.
- Fox, M., R. Reverman, F. Herman, M. G. Fellin, P. Sternai, and S. D. Willett (2014), Rock uplift and erosion rate history of the bergell intrusion from the inversion of low temperature thermochronometric data, *Geochemistry, Geophysics, Geosystems*, 15(4), 1235–1257.
- Fox, M., T. Bodin, and D. L. Shuster (2015), Abrupt changes in the rate of andean plateau uplift from reversible jump markov chain monte carlo inversion of river profiles, *Geomorphology*, 238, 1–14.
- Gallagher, K., K. Charvin, S. Nielsen, M. Sambridge, and J. Stephenson (2009), Markov chain monte carlo (mcmc) sampling methods to determine optimal models, model resolution and model choice for earth science problems, *Marine and Petroleum Geology*, 26(4), 525–535.
- Gasparini, N. M., and M. T. Brandon (2011), A generalized power law approximation for fluvial incision of bedrock channels, *Journal of Geophysical Research: Earth Surface*, 116(F2).
- Gelman, A., D. B. Rubin, et al. (1992), Inference from iterative simulation using multiple sequences, *Statistical science*, 7(4), 457–472.
- Geyer, C. J., and E. A. Thompson (1995), Annealing markov chain monte carlo with applications to ancestral inference, *Journal of the American Statistical Association*, 90(431), 909–920.
- Girolami, M., and B. Calderhead (2011), Riemann manifold langevin and hamiltonian monte carlo methods, *Journal of the Royal Statistical Society: Series B (Statistical Methodology)*, 73(2), 123–214.
- Godard, V., J. Lavé, and R. Cattin (2006), Numerical modelling of erosion processes in the himalayas of nepal: Effects of spatial variations of rock strength and precipitation, *Geological Society, London, Special Publications*, 253(1), 341–358.
- Goren, L., M. Fox, and S. D. Willett (2014), Tectonics from fluvial topography using formal linear inversion: Theory and applications to the inyo mountains, california, *Journal of Geophysical Research: Earth Surface*, 119(8), 1651–1681.
- Grandis, H., M. Menvielle, and M. Roussignol (1999), Bayesian inversion with markov chains—i. the magnetotelluric one-dimensional case, *Geophysical Journal International*, 138(3), 757–768.
- Haario, H., E. Saksman, J. Tamminen, et al. (2001), An adaptive metropolis algorithm, *Bernoulli*, 7(2), 223–242.
- Harel, M.-A., S. Mudd, and M. Attal (2016), Global analysis of the stream power law parameters based on worldwide 10be denudation rates, *Geomorphology*, 268, 184 – 196.
- Hastings, W. K. (1970), Monte carlo sampling methods using markov chains and their applications, *Biometrika*, 57(1), 97–109.
- Hobley, D. E., J. M. Adams, S. S. Nudurupati, E. W. Hutton, N. M. Gasparini, E. Istanbuloglu, and G. E. Tucker (2017), Creative computing with landlab: an open-source toolkit for building, coupling, and exploring two-dimensional numerical models of earth-surface dynamics, *Earth Surface Dynamics*, 5(1), 21.
- Hobley, D. E. J., H. D. Sinclair, S. M. Mudd, and P. A. Cowie (2011), Field calibration of sediment flux dependent river incision, *Journal of Geophysical Research: Earth Surface*, 116(F4).
- Hoffman, M. D., and A. Gelman (2014), The no-u-turn sampler: adaptively setting path lengths in hamiltonian monte carlo., *Journal of Machine Learning Research*, 15(1), 1593–1623.

- Howard, A. D., W. E. Dietrich, and M. A. Seidl (1994), Modeling fluvial erosion on regional to continental scales, *Journal of Geophysical Research: Solid Earth*, *99*(B7), 13,971–13,986.
- Karimi, K., N. Dickson, and F. Hamze (2011), High-performance physics simulations using multi-core cpus and gpgpus in a volunteer computing context, *The International Journal of High Performance Computing Applications*, *25*(1), 61–69.
- Kone, A., and D. A. Kofke (2005), Selection of temperature intervals for parallel-tempering simulations, *The Journal of chemical physics*, *122*(20), 206,101.
- Lamport, L. (1986), On interprocess communication, *Distributed computing*, *1*(2), 86–101.
- Li, Y., M. Mascagni, and A. Gorin (2009), A decentralized parallel implementation for parallel tempering algorithm, *Parallel Computing*, *35*(5), 269 – 283.
- Malinverno, A. (2002), Parsimonious bayesian markov chain monte carlo inversion in a nonlinear geophysical problem, *Geophysical Journal International*, *151*(3), 675–688.
- Maraschini, M., and S. Foti (2010), A monte carlo multimodal inversion of surface waves, *Geophysical Journal International*, *182*(3), 1557–1566.
- Marinari, E., and G. Parisi (1992), Simulated tempering: a new monte carlo scheme, *EPL (Europhysics Letters)*, *19*(6), 451.
- Metropolis, N., A. W. Rosenbluth, M. N. Rosenbluth, A. H. Teller, and E. Teller (1953), Equation of state calculations by fast computing machines, *The journal of chemical physics*, *21*(6), 1087–1092.
- Miasojedow, B., E. Moulines, and M. Vihola (2013), An adaptive parallel tempering algorithm, *Journal of Computational and Graphical Statistics*, *22*(3), 649–664.
- Mills, K., G. Fox, and R. Heimbach (1992), Implementing an intervisibility analysis model on a parallel computing system, *Computers & Geosciences*, *18*(8), 1047–1054.
- Mingas, G., L. Bottolo, and C.-S. Bouganis (2017), Particle mcmc algorithms and architectures for accelerating inference in state-space models, *International Journal of Approximate Reasoning*, *83*, 413–433.
- Mosegaard, K., and A. Tarantola (1995), Monte carlo sampling of solutions to inverse problems, *Journal of Geophysical Research: Solid Earth*, *100*(B7), 12,431–12,447.
- Mosegaard, K., and P. D. Vestergaard (1991), A simulated annealing approach to seismic model optimization with sparse prior information, *Geophysical Prospecting*, *39*(5), 599–611.
- Neal, R. M. (1996), Sampling from multimodal distributions using tempered transitions, *Statistics and computing*, *6*(4), 353–366.
- Neal, R. M., et al. (2011), Mcmc using hamiltonian dynamics, *Handbook of Markov Chain Monte Carlo*, *2*(11).
- Patriksson, A., and D. van der Spoel (2008), A temperature predictor for parallel tempering simulations, *Physical Chemistry Chemical Physics*, *10*(15), 2073–2077.
- Reid, A., E. V. Bonilla, L. McCalman, T. Rawling, and F. Ramos (2013), Bayesian joint inversions for the exploration of Earth resources, in *IJCAI*, pp. 2877–2884.
- Rejman, J., R. Turski, and J. Paluszek (1998), Spatial and temporal variations in erodibility of loess soil, *Soil and Tillage Research*, *46*(1-2), 61–68.
- Robert, C., and G. Casella (2011), A short history of markov chain monte carlo: Subjective recollections from incomplete data, *Statistical Science*, pp. 102–115.
- Roberts, G. G., and N. White (2010), Estimating uplift rate histories from river profiles using african examples, *Journal of Geophysical Research: Solid Earth*, *115*(B2).
- Rocca, P., M. Benedetti, M. Donelli, D. Franceschini, and A. Massa (2009), Evolutionary optimization as applied to inverse scattering problems, *Inverse Problems*, *25*(12), 123,003.

- Salinger, M. (1980), New zealand climate: I. precipitation patterns, *Monthly weather review*, 108(11), 1892–1904.
- Salles, T. (2016), Badlands: A parallel basin and landscape dynamics model, *SoftwareX*, 5, 195–202.
- Salles, T., and G. Duclaux (2015), Combined hillslope diffusion and sediment transport simulation applied to landscape dynamics modelling., *Earth Surf. Process Landf.*, 40(6), 823–39.
- Salles, T., and L. Hardiman (2016), Badlands: An open-source, flexible and parallel framework to study landscape dynamics, *Computers & Geosciences*, 91, 77–89.
- Salles, T., N. Flament, and D. Müller (2017), Influence of mantle flow on the drainage of eastern australia since the jurassic period, *Geochemistry, Geophysics, Geosystems*, 18(1), 280–305.
- Salles, T., X. Ding, and G. Brocard (2018a), pybadlands: A framework to simulate sediment transport, landscape dynamics and basin stratigraphic evolution through space and time, *PloS one*, 13(4), e0195557.
- Salles, T., X. Ding, and G. Brocard (2018b), pybadlands: A framework to simulate sediment transport, landscape dynamics and basin stratigraphic evolution through space and time, *PLOS ONE*, 13, 1–24.
- Salles, T., X. Ding, J. M. Webster, A. Vila-Concejo, G. Brocard, and J. Pall (2018c), A unified framework for modelling sediment fate from source to sink and its interactions with reef systems over geological times, *Scientific Reports*, 8(1), 5252, doi:10.1038/s41598-018-23519-8.
- Sambridge, M. (1999), Geophysical inversion with a neighbourhood algorithm—ii. appraising the ensemble, *Geophysical Journal International*, 138(3), 727–746.
- Sambridge, M. (2013), A parallel tempering algorithm for probabilistic sampling and multimodal optimization, *Geophysical Journal International*, 196(1), 357–374.
- Sambridge, M., and K. Mosegaard (2002), Monte carlo methods in geophysical inverse problems, *Reviews of Geophysics*, 40(3).
- Scalzo, R., D. Kohn, H. Olierook, G. Houseman, R. Chandra, M. Girolami, and S. Cripps (2019), Efficiency and robustness in monte carlo sampling for 3-d geophysical inversions with obsidian v0.1.2: setting up for success, *Geoscientific Model Development*, 12(7), 2941–2960, doi:10.5194/gmd-12-2941-2019.
- Scott, L. R., and S. Zhang (1990), Finite element interpolation of nonsmooth functions satisfying boundary conditions, *Mathematics of Computation*, 54(190), 483–493.
- Sen, M. K., and P. L. Stoffa (1996), Bayesian inference, gibbs’ sampler and uncertainty estimation in geophysical inversion, *Geophysical Prospecting*, 44(2), 313–350.
- Sen, M. K., and P. L. Stoffa (2013), *Global optimization methods in geophysical inversion*, Cambridge University Press.
- Stock, J. D., and D. R. Montgomery (1999), Geologic constraints on bedrock river incision using the stream power law, *Journal of Geophysical Research: Solid Earth*, 104(B3), 4983–4993.
- Tarantola, A. (2006), Popper, bayes and the inverse problem, *Nature physics*, 2(8), 492.
- Ter Braak, C. J. (2006), A markov chain monte carlo version of the genetic algorithm differential evolution: easy bayesian computing for real parameter spaces, *Statistics and Computing*, 16(3), 239–249.
- Tucker, G. E., and G. R. Hancock (2010), Modelling landscape evolution, *Earth Surface Processes and Landforms*, 35(1), 28–50.
- Ummenhofer, C. C., and M. H. England (2007), Interannual extremes in new zealand precipitation linked to modes of southern hemisphere climate variability, *Journal of Climate*, 20(21), 5418–5440.

- Vrugt, J. A., B. O. Nualláin, B. A. Robinson, W. Bouten, S. C. Dekker, and P. M. Soot (2006), Application of parallel computing to stochastic parameter estimation in environmental models, *Computers & Geosciences*, *32*(8), 1139–1155.
- Whipple, K. X., and G. E. Tucker (2002), Implications of sediment-flux-dependent river incision models for landscape evolution, *Journal of Geophysical Research: Solid Earth*, *107*(B2), 1–20.
- Zhang, H., M. Liu, Y. Shi, D. A. Yuen, Z. Yan, and G. Liang (2007), Toward an automated parallel computing environment for geosciences, *Physics of the Earth and Planetary Interiors*, *163*(1-4), 2–22.

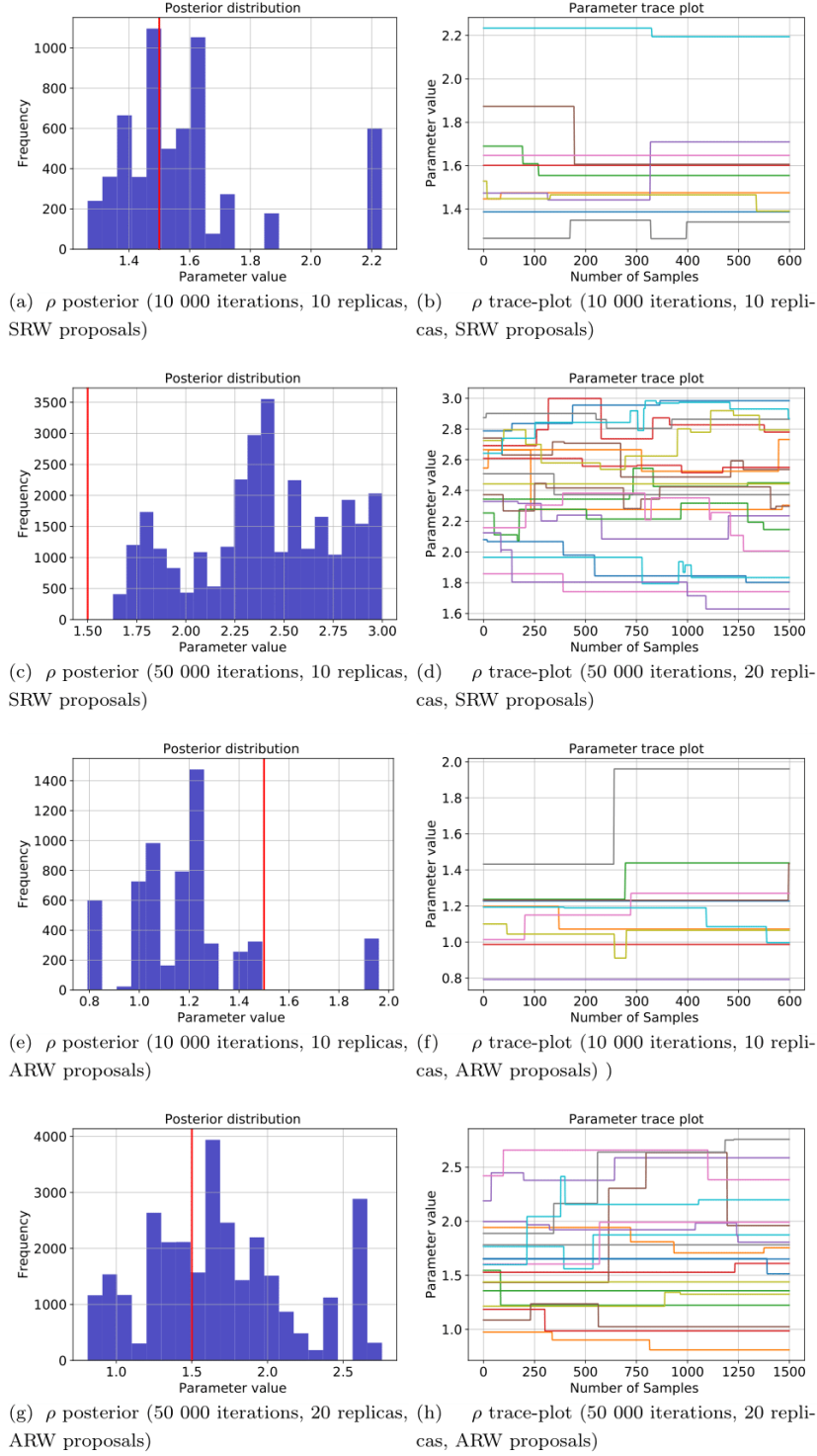


Figure 18: Posterior distribution and trace-plot during sampling for precipitation (ρ) parameter for different sampling times for the Cr problem using SRW and ARW proposal distributions in PT-Bayeslands. Panels (a) and (b) correspond to 10000 iterations with a SRW proposal. Panels (c) and (d) correspond to 50000 iterations with a SRW proposal. Panels (e) and (f) correspond to 10000 iterations with an ARW proposal and panels (g) and (h) correspond to 50000 iterations with an ARW proposal.

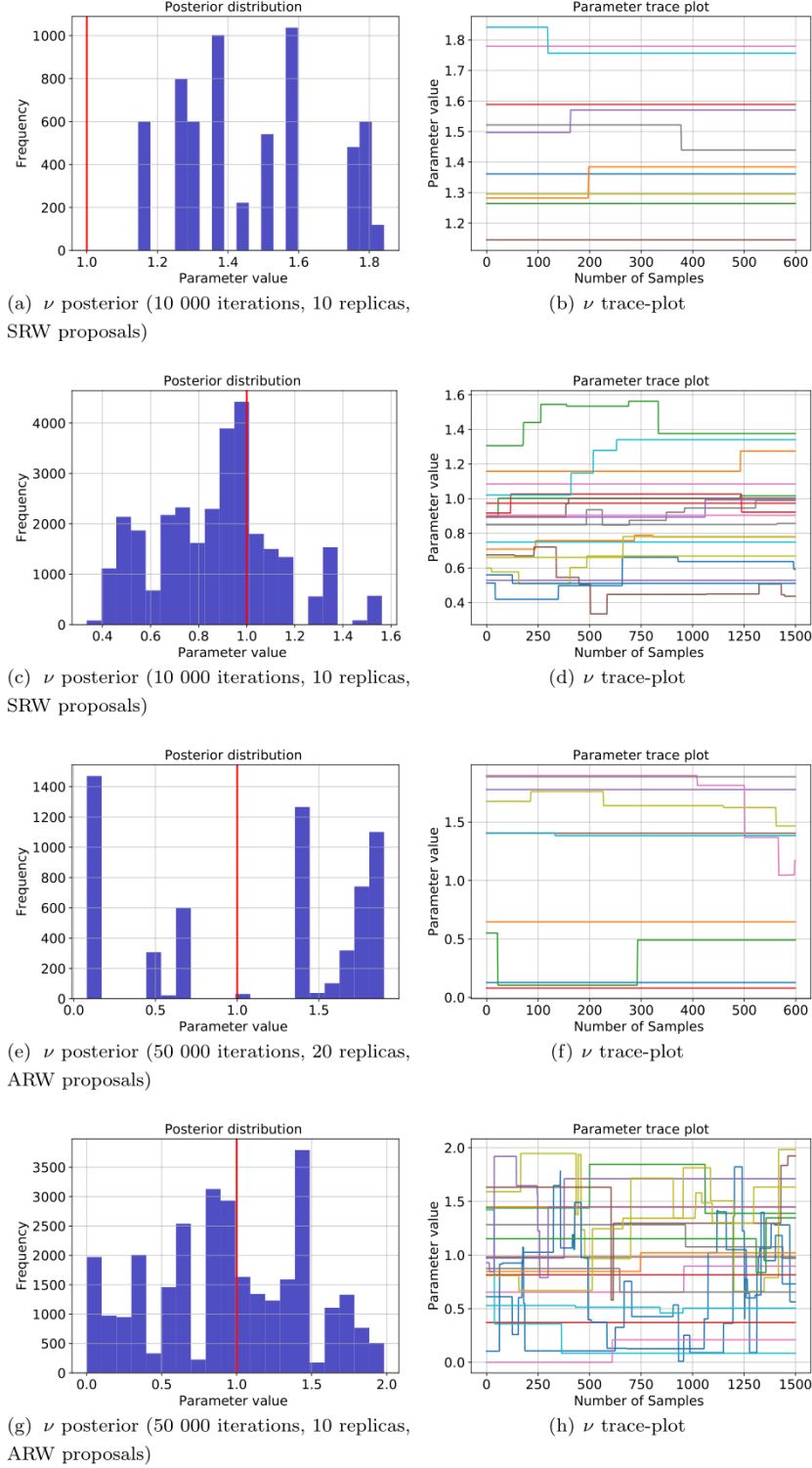


Figure 19: Posterior distribution and trace-plot during sampling for n -value (ν) parameter for different sampling times for the Cr problem using SRW and ARW proposal distributions in PT-Bayeslands. Panels (a) and (b) correspond to 10000 iterations with a SRW proposal. Panels (c) and (d) correspond to 50000 iterations with a SRW proposal. Panels (e) and (f) correspond to 10 000 iterations with an ARW proposal and panels (g) and (h) correspond to 50 000 iterations with an ARW proposal.

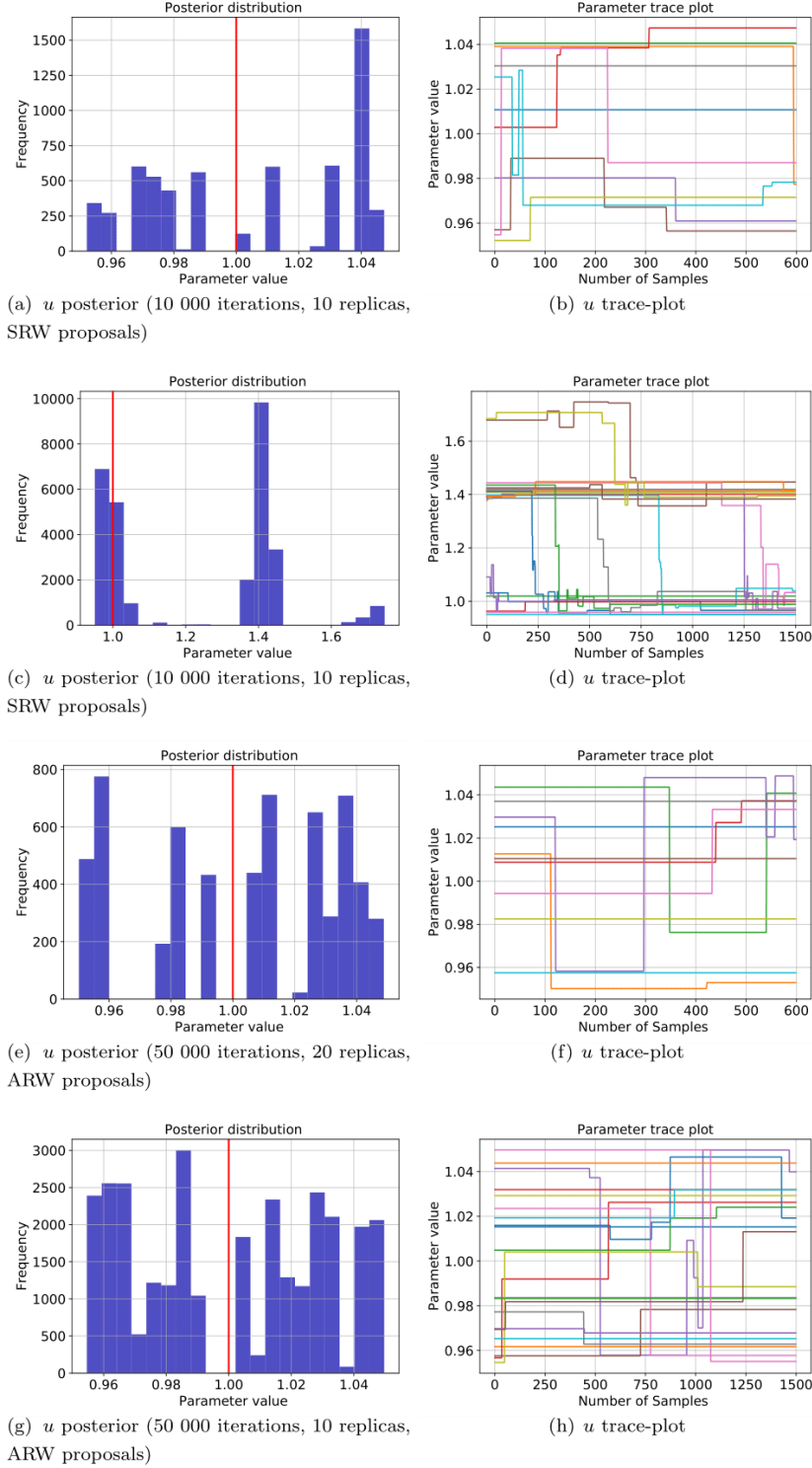


Figure 20: Posterior distribution and trace-plot during sampling for uplift (u) parameter for different sampling times for the Cr problem using SRW and ARW proposal distributions in PT-Bayeslands. Panels (a) and (b) correspond to 10000 iterations with a SRW proposal. Panels (c) and (d) correspond to 50000 iterations with a SRW proposal. Panels (e) and (f) correspond to 10 000 iterations with an ARW proposal and panels (g) and (h) correspond to 50 000 iterations with an ARW proposal.

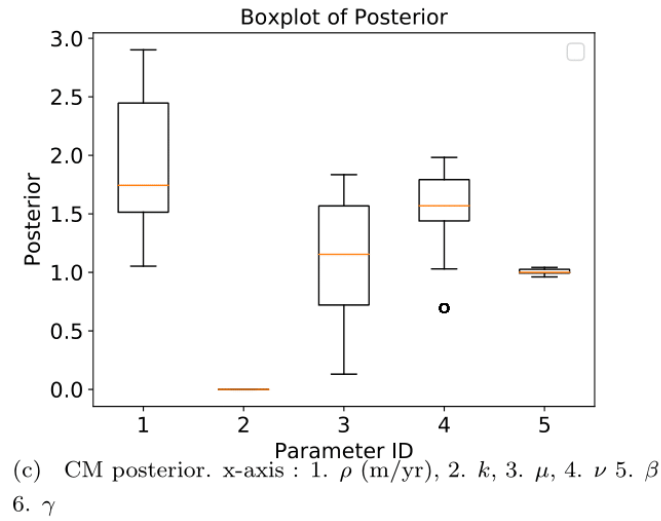
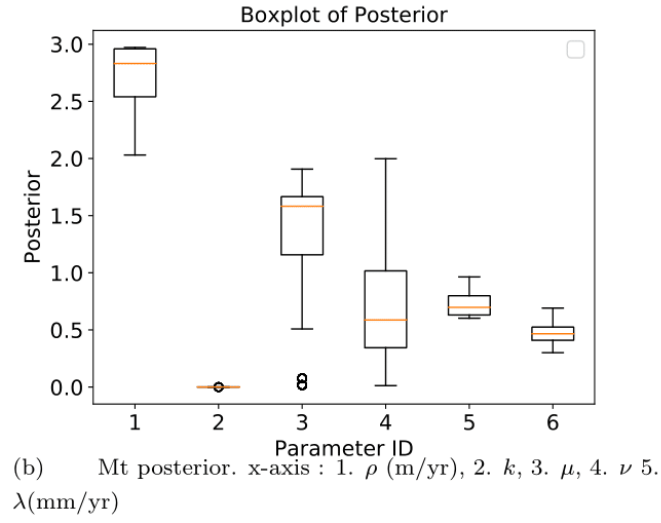
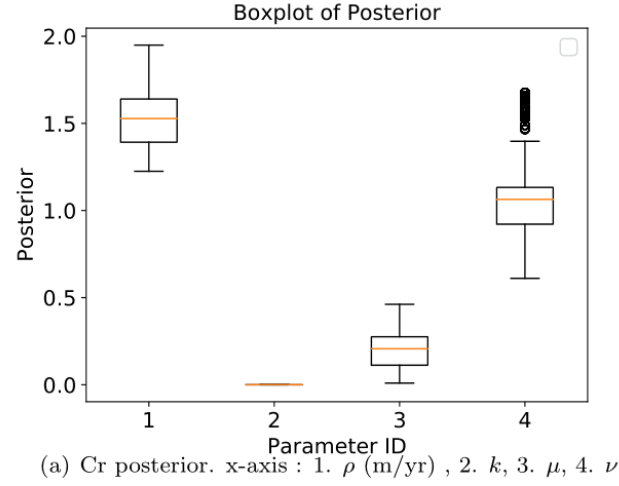
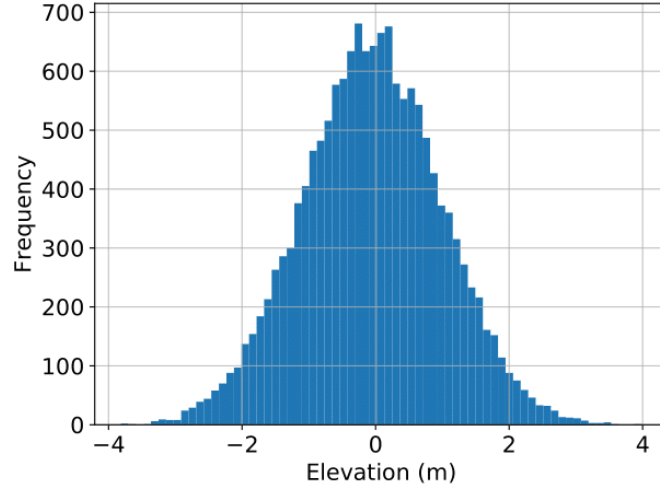
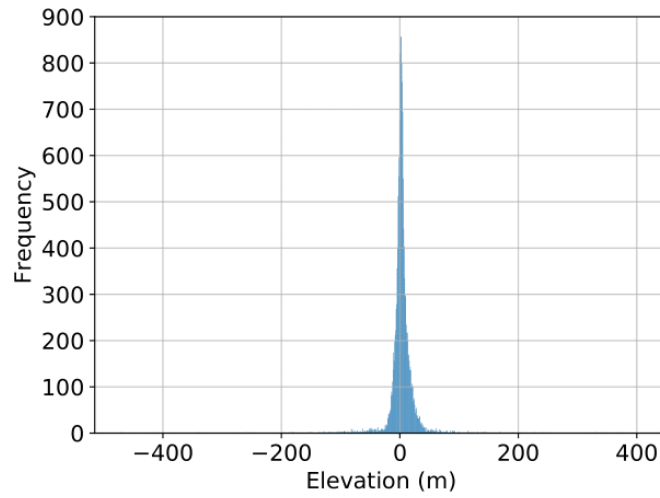


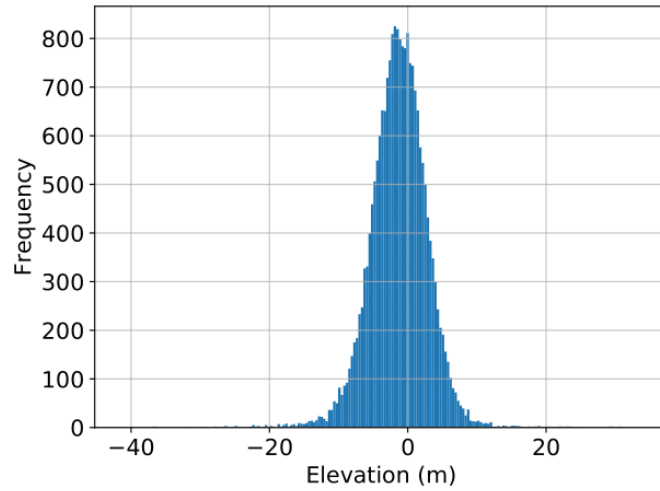
Figure 21: Boxplot showing the posterior distribution of the free parameters for the respective problems.



(a) Cr topography



(b) CM topography



(c) Mt topography

Figure 22: Distribution of topography residuals for the respective problems (Cr, Mt and CM)